AN ABSTRACT OF THE THESIS OF

Dennise M. Magill for the degree of Master of Science in Radiation Health Physics presented on September 8, 2010.

Title: Radiation Dose and Risk in Interventional Neuroradiology.

Abstract approved:

_____

Camille Lodwick

BACKGROUND/PURPOSE: Exposure from medical radiation sources are on the rise in the United States. Often the highest potential source of radiation dose to patients and radiology staff occur during interventional radiology procedures performed using fluoroscopy and digital subtraction angiography (DSA) to provide image guidance in minimally invasive surgical procedures. Several methods have been proposed for monitoring these radiation doses. The radiology staff are legally required by the Nuclear Regulatory Commission (NRC), or Agreement States, to wear radiation dosimetry badges on the outside of their lead aprons, but at this time the only patient dose requirements are equipment based monitors with audible alarms. Interventional patient radiation dose monitoring has not been standardized for all institutions performing these procedures, so it is the responsibility of the institution and thus the Interventionalist performing the procedure to be aware of the patient radiation dose and potential risks associated with that dose during the procedure.

MATERIALS/METHOD: An investigation of Interventional Neuroradiology (INR) patient cases performed during a one month period beginning in February 2010 at the Medical University of South Carolina (MUSC) were studied to characterize the typical radiation geometries, and general patient demographic (ie. sex and age) for these procedures. Using that knowledge effective dose and thyroid dose conversion factors were derived for use in calculating patient radiation doses post procedure. A relationship between the thyroid organ dose and consequent risk of thyroid cancer incidence was established using the BEIR VII data.

RESULTS: Sample calculations were completed on a small cohort of these INR patients undergoing both treatment and diagnostic procedures with fluoroscopy times averaging 49 minutes. Using the conversion factors established from the typical INR radiation geometries effective doses ranged from 0.23 mSv to 1.49 mSv and thyroid organ doses ranged from 0.35 mGy to 4.56 mGy. The corresponding risk of thyroid cancer incidence was greatest for adult females age 25 by a factor of ~ 5 to that of their male counterparts. The difference in age from 25 to 65 years decreases the thyroid cancer incidence risk by a factor of ~ 83 in females and ~ 58 in males.

CONCLUSION: The ability to quantify the radiation dose imparted to the patient during an INR procedure and the associated cancer incidence risk is essential to establishing effective radiation safety guidelines and monitoring methods within an institution.

Radiation Dose and Risk in Interventional Neuroradiology

by
Dennise M. Magill

A THESIS

submitted to

Oregon State University

in partial fulfillment of
the requirements for the
degree of

Master of Science

Presented September 8, 2010
Commencement June 2011

Master of Science thesis of Dennise M. Magill
presented on September 8, 2010.

APPROVED:

_____

Major Professor, representing Radiation Health Physics

_____

Head of the Department of Nuclear Engineering and Radiation Health Physics

_____

Dean of the Graduate School

I understand that my thesis will become part of the permanent collection of Oregon State University libraries. My signature below authorizes release of my thesis to any reader upon request.

_____

Dennise M. Magill, Author

ACKNOWLEDGEMENTS

The author expresses sincere appreciation to Walter Huda PhD. and the departments of Radiological Science and Neurointerventional Radiology at the Medical University of South Carolina. This research project was made possible through Dr. Huda's continual guidance and mentorship. His approach to research inspires a sense of scientific adventure and is a constant source of education.

The author would also like to express gratitude to Camille Lodwick PhD. at Oregon State University Department of Nuclear Engineering and Radiation Health Physics for serving as an advisor for this master's thesis project. Dr. Lodwick's patience and support were greatly appreciated during this process.

TABLE OF CONTENTS

TABLE OF CONTENTS (continued)

LIST OF FIGURES

LIST OF FIGURES (Continued)

Figure Page

LIST OF TABLES

LIST OF ACRONYMS

Acronym	Definition
ACR	American College of Radiology
ASTIN	American Society of Interventional and Therapeutic Neuroradiology
AVM	Arteriovenous Malformation
BEIR	Biological Effects of Ionizing Radiation
CAUD	Caudial Image Projection Tilt
CFR	Code of Federal Regulations
CRAN	Cranial Image Projection Tilt
DAP	Dose Area Product ($mGy \cdot cm^2$)
DSA	Digital Subtraction Angiography
D_T	Thyroid Organ Dose (mGy)
ED	Effective Dose (E)
FDA	US Food and Drug Administration
FSD	Focal Spot to Source Distance
GDC	Guglielmi Detachable Coil
ICRP	International Commission on Radiological Protection
IEC	The International Electrotechnical Commission
INR	Interventional Neuroradiology
IR	Interventional Radiology
IRP	Interventional Reference Point
KAP	Kerma Area Product
LAO	Left Anterior Oblique Image Projection
LET	Linear Energy Transfer ($keV \cdot \mu m^{-1}$)
NCRP	National Council on Radiological Protection and Measurements
RAO	Right Anterior Oblique Image Projection

RSNA	Radiological Society of North America
SID	Source to Image Distance
SNIS	Society of Neurointerventional Surgery
SSD	Source to Skin Distance
UNSCEAR	United Nations Scientific Committee on the Effects of Atomic Radiation

Radiation Dose and Risk in Interventional Neuroradiology

1. INTRODUCTION

1.1. Interventional Radiology

Interventional Radiology (IR) is defined by the American College of Radiology (ACR) in conjunction with the Radiological Society of North America (RSNA) as, "the clinical subspecialty that uses fluoroscopy, CT, and ultrasound to guide percutaneous (through the skin) procedures such as performing biopsies, draining fluids, inserting catheters, or dilating or stenting narrowed ducts or vessels."[1] IR was originally pioneered by Charles Dotter in the 1960's when he began lecturing about it, and performed the first angioplasty procedure as a percutaneous dilation of an 82 year old woman's localized stenosis of her superficial femoral artery by placing an arterial coaxial Teflon catheter on January 16, 1964.[2] In 1978 Dr. Dotter was awarded the Nobel Prize in medicine and is considered the "Father of Interventional Radiology."[3] The Society of Interventional Radiology was formed in 1973 and currently has over 4,500 professional members.[4]

IR procedures now encompass an expanding range of sub-specialties from general IR to cardiac catheterization, electrophysiology procedures, pain management, radiation oncology applications, neuroradiology, pediatrics, musculoskeletal, etcetera. There are a broad spectrum of surgical procedures that utilize image guidance. The advances in IR technique allow for less invasive, generally more cost efficient surgeries, which often provide a better prognosis than traditional surgery.[4-5] According to a guidance report by the ACR these procedures can be conducted in both outpatient clinics as well as in the traditional hospital

environment.[6] Image guided surgeries use a variety of modalities such as fluoroscopy, computed tomography (CT), ultrasound and magnetic resonance imaging (MRI); however, the largest potential radiation dose in IR is with fluoroscopic exposures. In 2009, fluoroscopic exposures during IR procedures were the third largest source of medical radiation, outranked only by CT and Nuclear Medicine. Fluoroscopy currently contributes to 14% of the total medical radiation to the public in the United States.[7]

The total amount of radiation incident on a patient during an IR procedure fluctuates dependent on the actual complexity of the various procedures and the imaging needs for the individual patient's anatomy. Longer fluoroscopic exposure times will increase the radiation dose to both the patient and the staff. Furthermore, the patient skin dose will be intensified with imaging area reduction and concentration in a particular anatomical region.[5] Absorbed skin doses can range from 20 mGy min^{-1} to greater than 50 mGy min^{-1} in typical IR procedures, and effective doses can be on the order of 1 mSv to 50 mSv for lengthy, or complicated, procedures.[7]

1.2. Focusing on Interventional Neuroradiology

Between 2002 and 2004 the National Council on Radiation Protection and Measurements (NCRP) estimated a 54% increase in all IR procedures, and the Society of Neurointerventional Surgery (SNIS formerly ASTIN) estimated a 48% annual growth in procedures in 2006.[7-8] Due to the growth rate of IR procedures it was evident that this research would need to focus on one IR subspecialty in order to adequately characterize the patients, radiation geometry and resulting radiation doses and cancer risks.

2. BACKGROUND / LITERATURE REVIEW

2.1. Interventional Neuroradiology

Interventional Neuroradiology (INR) is an IR subspecialty in which percutaneous puncture of the cerebral artery is performed to insert a catheter for injection of a contrast medium for vascular imaging in the head and neck regions. The diagnostic technique, cerebral angiography, was first performed on cadavers in 1896 and by the 1960's this imaging technique had become the gold standard for intracranial imaging.[9] INR currently encompasses not only diagnostic intracranial imaging, but also therapeutic intracranial procedures. The procedures performed in INR can be distinctly categorized as either diagnostic or therapeutic.

2.1.1. Diagnostic Procedures

INR diagnostic procedures, cerebral angiography, are among the most basic procedures performed in INR. The purpose of cerebral angiography is to simply provide reliable images of cerebrovascular structures. The indications for these procedures include diagnosis of neurovascular disease, planning for INR treatment (which may be completed just prior to the treatment commencement), and as post treatment follow up imaging. The typical neurovascular diseases diagnosed through cerebral angiography are aneurysm, arteriovenous malformation (AVM), dural arteriovenous fistulas, atherosclerotic stenosis, vasculopathy, cerebral vasospasm, and acute ischemic stroke.[9]

Neurological complications resulting from cerebral angiography are rare, occurring in ~1.3% of cases.[10] A majority of these complications are

reversible carotid ischemic events due to thromboembolism or air emboli from catheter injections. Non-neurological complications are also relatively rare. Commonly the femoral artery is used as the access point, so non-neurological complications may consist of groin and retroperitoneal hematomas, pseudoaneurysm of the femoral artery, and lower extremity thromboembolism. The contrast medium can also introduce the possibility of allergic reactions, and renal complications. These complications are each <1% occurrence in diagnostic INR cases.[11]

2.1.2. Therapeutic Procedures

Therapeutic procedures are an extension of the diagnostic procedure when a medical intervention of the abnormality is also completed during the procedure. Therapeutic procedures will be categorized as stroke therapy, aneurysm therapy, AVM, and miscellaneous therapies since these are the most plausible categorical organization of the procedures used in this study at MUSC.

2.1.2.1. Stroke Therapy

Acute ischemic stroke occurs from a blockage in a blood vessel, which prevents oxygenated blood from reaching the tissues supplied by the vessel. The blockage is generally the result of a cardiogenic embolism, artherosclerosis, thrombosis, or an arterial disease such as lipophyalinosis.[12] Stroke victims can be treated with either intravenous (IV) or intra-arterial (IA) thrombolysis. The later technique yields a greater recanalization rate of 70% versus 34% with the former technique.[12-13]

In IV therapy a thrombolytic drug is administered through a venous access point usually located in the antecubital arm, forearm, wrist, or hand. The IA technique delivers a similar thrombolytic pharmaceutical directly to

the stroke site, so it does not have travel through the patient's circulatory system, and the entire dose is concentrated in the blockage. The ideal time frame to initiate IA stroke therapy is within 6 hours of the onset of the patient's symptoms. Although successful therapies have been recorded at up to 48 hours.[13]

2.1.2.2. Aneurysm Therapy

Intracranial aneurysms occur in approximately 8% of the population.[14] INR can be used to treat subarachnoid hemorrhage, and un-ruptured intracranial aneurysms by constructive (coiling) or deconstructive (clipping) treatment methods. The alternative is a clipping of the aneurysm via craniotomy, so INR provides a less invasive method of treatment. With either method (INR or craniotomy) the goal is to completely obliterate the aneurismal dome and sac.

INR constructive treatment, or coiling, allows a reconstruction of the vessel lumen to reestablish the original blood flow and preserve the patient's vasculature.[12] A catheter and guide wire are inserted through the femoral artery and advanced to the level of the aneurysm using fluoroscopic imaging to ensure safety and accuracy of the catheter. The Guglielmi detachable coil (GDC) embolization is the most commonly used technique where a GDC coil attached to a delivery wire is inserted into the catheter and advanced to the level of the aneurysm.[12] Fluoroscopy is used to provide real time imaging of the coil placement in the aneurismal dome and to ensure that the coil does not impede the patient's normal blood flow through the lumen. Since the coil is attached to the delivery wire it can be removed if a different size is needed, or repositioned in the aneurysm. When the coil is appropriately placed an electrical current with a low

amplitude is applied to the dissolve the solder joint between the delivery wire and the coil.[12]

Deconstructive treatment, or clipping, sacrifices the vasculature of the vessel containing the aneurysm. Basically instead of blocking the aneurysm this method blocks the entire vessel. If the patient is a candidate for a craniotomy a surgical clip is placed in the region of the aneurysm. In INR clipping treatment two devices are implanted into the neck of the aneurysm (or vessel lumen) both inferiorly and distally to the aneurysm.[14] These devices create a blockage in the vessel that inhibits the natural blood flow through the vessel in the area of the aneurysm.

2.1.2.3. Arteriovenous Malformation

Arteriovenous malformations have been difficult to successfully treat without causing substantial risk to the patient. INR techniques have become incredibly valuable in the treatment of AVM's due to technological advancements in catheters and embolic agents resulting in a treatment that is more effective and safer for the patient.[15]

An AVM consists of a malformation of the vessel walls of an artery and vein in the brain. Essentially the artery and vein are connected without the normal intermediary capillary system, so the arterial and venous blood flow are freely exchanged causing a decrease in the oxygenated blood available to the tissue supplied by the artery. Adults ages 20 to 40 presenting with headache, seizures, or brain hemorrhage may suffer from this disorder, and AVM hemorrhage carries a mortality rate of ~10%.[15] AVM is diagnosed by a variety of imaging techniques including CT, MRI, MRA, and diagnostic cerebral angiography.[16]

AVM's are treated in INR with embolotherapy where a catheter is advanced from the external venous access point to the intracranial AVM to administer an embolic agent with the purpose of obliterating the vessel inferiorly and distal to the AVM to prevent future blood shunting. Embolotherapy is performed exclusively with two types of microcatheters. The first type is a small catheter with a guide wire for advancement and the second uses the arterial blood flow to carry the catheter to the AVM. Once the catheter reaches the AVM an embolic agent, such as particles, coils, balloons, and/or liquids, are administered through the catheter to block the malformed vessels.

2.1.2.4. Miscellaneous Therapies

The therapies that were designated to the miscellaneous category is this study consisted of sclerotherapy, vasospasms, and a few pediatric case. The pediatric cases were not in the scope of this study, therefore, the miscellaneous therapies will refer to sclerotherapy and cerebral vasospasm therapy procedures in adults.

Sclerotherapy can be used to treat some AVM's by accessing the AVM through the venous route as opposed to the arterial route, which can be more complicated. Once the catheter is in place a sclerotic agent (absolute ethanol, or *n*-butyl cyanoacrylate (NBCA)) is administered to effectively create a chemical embolization of the AVM.[17-18]

Cerebral vasospasm is the arterial narrowing consistent with slow filling contrast agent visualized in diagnostic angiography images, and usually arise as a result of post aneurismal subarachnoid hemorrhage (SAH).[19] Endovascular treatment of this condition involves the use of a catheter that a balloon can be advanced through to the affected region of

the artery. The balloon is inflated in this region and counteracts the vasospasm to expand the vessel. Once the vasospasm is relaxed the balloon is deflated and removed through the catheter.[20]

2.2 MUSC INR Patient Population

INR patients are generally a mixture of adult and pediatric ages depending on the disease process being treated or imaged. A sampling of all the INR cases at the Medical University of South Carolina for February 2010 yielded a total of 75 cases with the majority being adults over the age of 25. Table 1 shows the demographic data (ie. age and gender) of this group. Seven of these patients were considered pediatric (under the age of 18) and therefore excluded from this study. The adult patients ranged in age from 25 to 86, and the youngest patients are seen in the AVM, diagnostic, and miscellaneous procedure categories.

Table 1. February 2010 MUSC INR case gender and age (years) demographics.

Exam	Male	Female	Total	Age	
				Minimum	Maximum
Aneurysm	5	13	18	28	86
AVM	1	3	4	14	43
Diagnostic	15	20	35	14	81
Stroke	4	4	8	51	83
Miscellaneous	3	4	7	1	81
All Exams	29	46	75	1	86

Figure 1 is a histogram of the adult male and female INR patient population during the same time frame at MUSC. A majority (~88%) of these patients were over the age of 40.

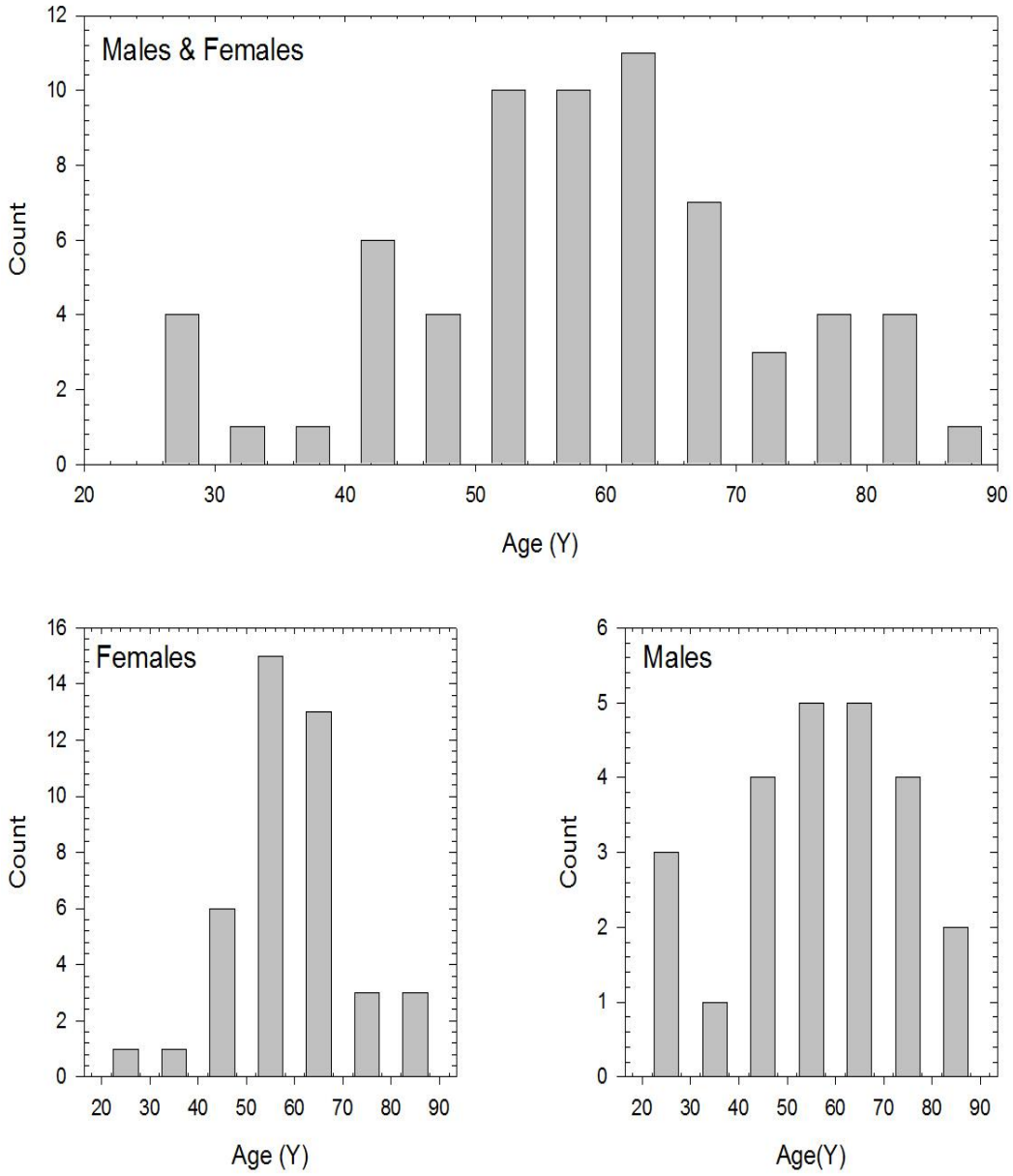

Figure 1. MUSC patient age histogram for Neuroradiology procedures performed during February 2010.

2.3. Imaging: Equipment, Acquisition and Radiation Monitoring

2.3.1. Siemens Axiom Artis BA

The INR laboratory at MUSC currently uses the Siemens Axiom Artis BA manufactured in Germany in May 2004 and installed at MUSC in July 2004. The Axiom Artis BA is a biplane C-arm consisting of both floor mounted and ceiling mounted C-arms as illustrated below in Figure 2.

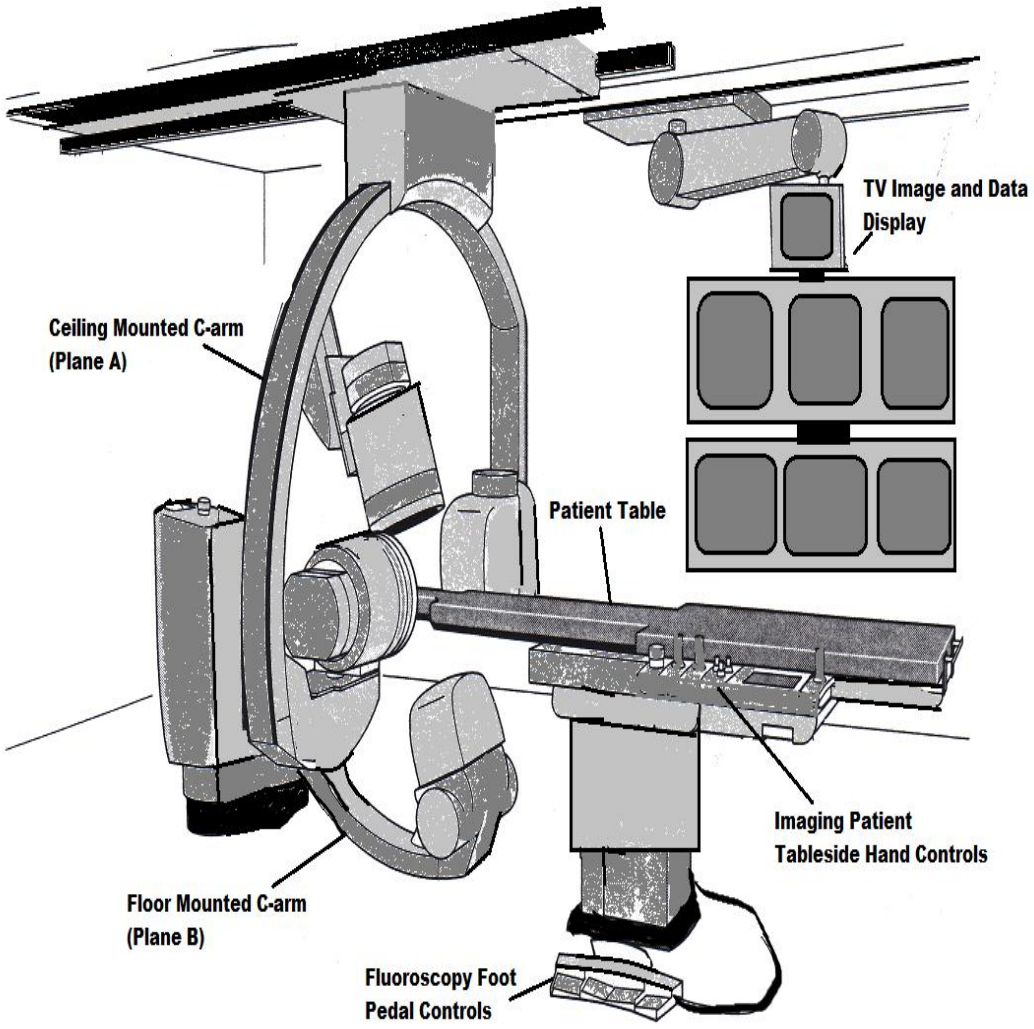

Figure 2. Schematic of the Siemens Axiom Artis BA biplane interventional suite used for both INR diagnostic and treatment procedures.*(Adapted from Siemens Artis BA Manual)*[21]

The unit has an x-ray generator with a nominal power of 80 kW (100 kV, 80 mAs) and a Megalix Cat 125/15/40/80-121 GW x-ray tube assembly. The power supply is a three phase current with a power distributor voltage of 380 V to 480 V ±10% at a frequency of 50 Hz to 60 Hz and a power consumption of 10 kVA. The Megalix Cat 125/15/40/80-121 GW x-ray tube is a "high performance x-ray tube with a metal center tube using liquid bearing technology and constant anode rotation."[21] The x-ray tube anode angle is 12° with a heat storage capacity of 1.4 MJ (2.0 MHU), and a three phase current anode drive of 150 Hz. The recommended operating temperature for this unit is 22 °C (72 °F). There are three focal spot sizes (micro 0.3 mm, small 0.6 mm, and large 1.0 mm) with a maximum voltage of 125 kV. The leakage radiation measurement according to Siemens at 1 m away from the housing is <0.35 mGy/h at the maximum voltage.

Each C-arm houses a Sirecon HDR image intensifier (II) opposite the x-ray tube assembly. The ceiling mounted C-arm has 5 zoom levels with II diameters (cm) of 11, 16, 22, 32 and 48, and an II diameter (cm) of 42 in Digital Subtraction Angiography (DSA) mode. The floor mounted C-arm has 4 zoom levels with II diameters (cm) of 10, 16, 20, and 25. The resolution is measured in line pairs per mm (lp/mm) and increases as the diameter size decreases. The resolution for each II diameter ranges from 4.2 lp/mm to 6.6 lp/mm. Figure 3 illustrates the configuration of x-ray tube and II in the two C-arms.

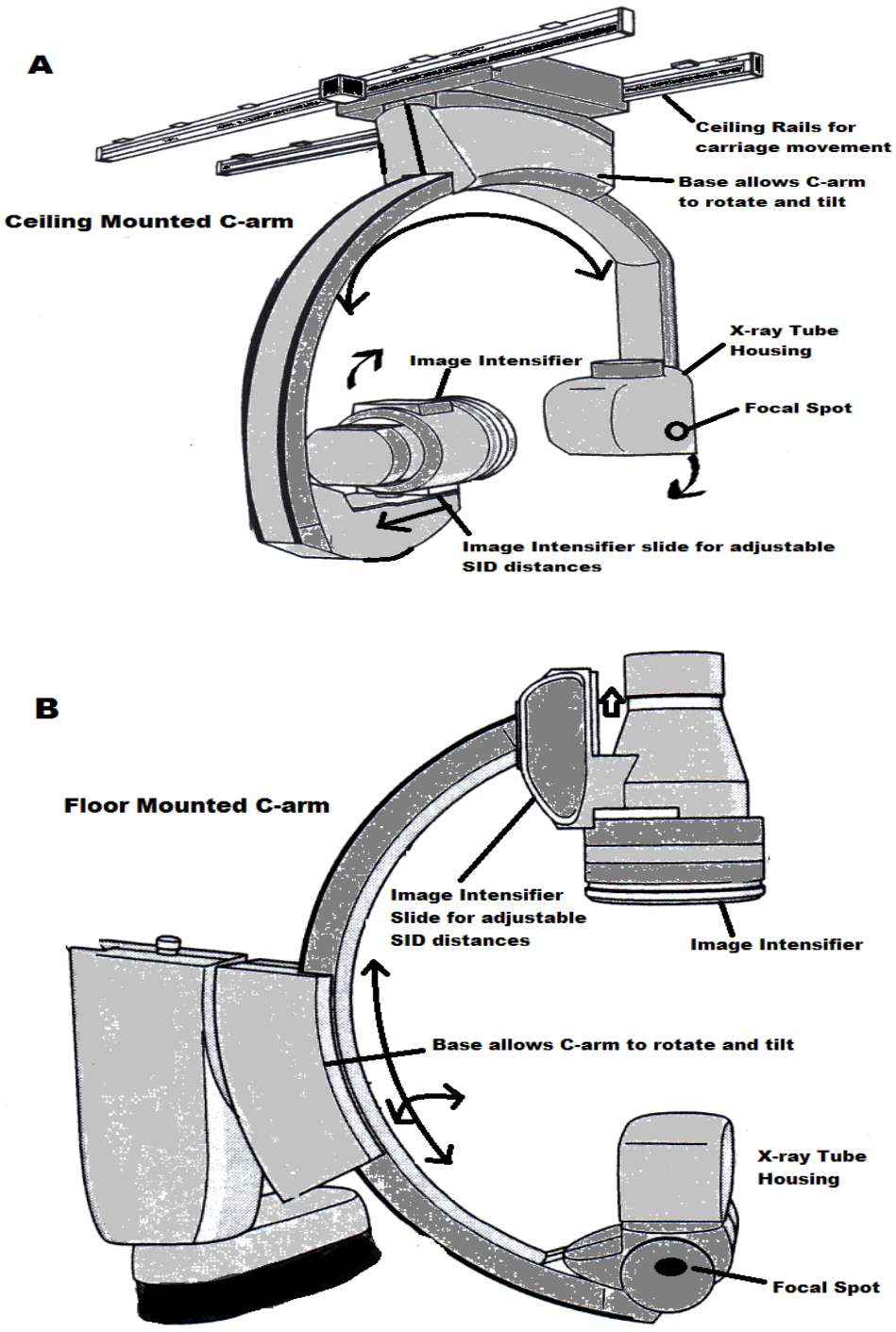

Figure 3. Diagram of the (A) ceiling mounted C-arm and (B) Floor mounted C-arm. ***(Adapted from Siemens Axiom Artis BA Manual)***[21]

These two C-arms move independently and are controlled by the operator for imaging in the posteroanterior and lateral projections. Plane A is assigned to the ceiling mount and Plane B is the floor mounted C-arm. During imaging the patient is isocentered in the x-ray beam, so that the middle of the patient's body coincides with the midpoint between the x-ray tube and the II. 15 cm from the isocenter in the direction of the x-ray tube, is the Interventional Reference Point (IRP) which will be discussed later in this chapter, but is illustrated in Figure 4.

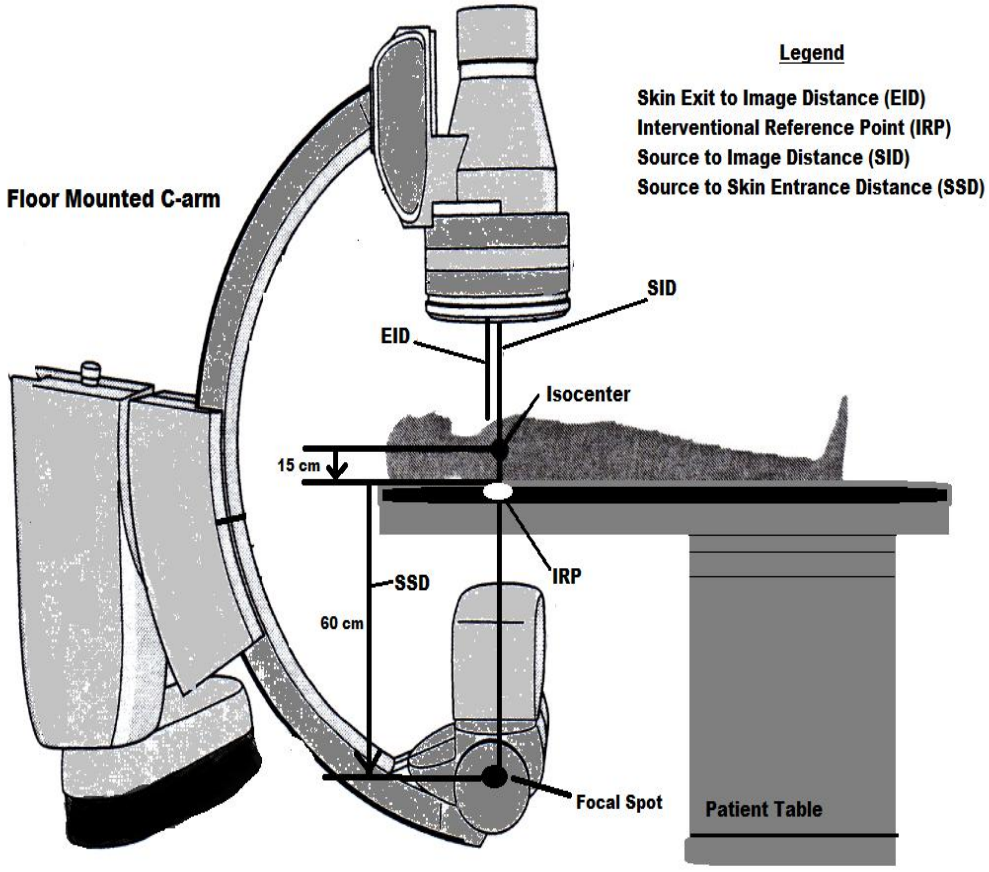

Figure 4. The radiation dose values are all measured at a distance 15 cm from the isocenter in the direction of the x-ray tube assembly, which is also shown as the equivalent to 60 cm from the x-ray tube focal spot. Several other field measurements are also depicted. ***(Adapted from Siemens Axiom Artis BA Manual)***[21]

2.3.2. Imaging Acquisition

2.3.2.1. Fluoroscopy

Fluoroscopy is real time x-ray technology, which utilizes an x-ray tube mounted to a C shaped gantry opposite of an image intensifier (II). X-ray's are generated through thermionic emission of electrons from a cathode and focused towards a rotating anode target in an evacuated glass envelope. These electrons travel from the cathode to a spinning beveled anode where the electrons will interact with the anode material to create both characteristic and Bremsstrahlung x-rays as shown in Figure 5.

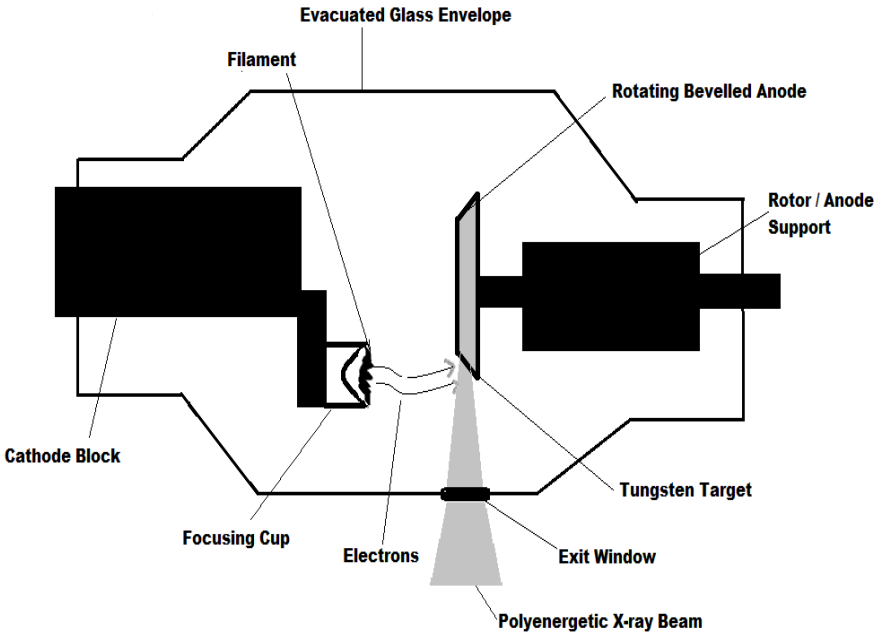

Figure 5. Diagram of a rotating anode x-ray tube assembly. ***(Adapted from W. Huda, 2010)***[22]

As the x-rays transmit through the exit window of the x-ray tube assembly they will be collimated to reduce scatter by focusing the beam and to account for the heel effect.

The resultant beam is poly-energetic due to the electrons and x-rays having travelled various distances in the anode material. This means that certain areas of the beam will be predisposed to higher energies than other areas resulting in a non-uniform beam. Collimation aides in reducing the low energy x-rays that will only contribute to the patient dose and creates an x-ray beam that is energetically more uniform (this is also known as beam hardening). Only about 1% of the incident x-rays will transmit through the patient to the II. Roughly 60% will be scattered from the patient and will not contribute to the image, and the rest will be absorbed by the patient.

The purpose of the II is to convert the transmitted x-rays into light photons and to achieve a flux and minification gain. The II has a curved vacuum window that creates both mechanical stability and strength. The window is thin so as not to absorb the x-rays as they are transmitted to the input phosphor. The input phosphor converts the x-rays into light photons and is generally made of a material that has a k-edge in the range of 30-40 keV such as Cesium Iodide (CsI). The resultant light photons are passed through a photocathode that converts the light photons into low energy electrons. A high voltage power supply is applied between the photocathode and the output phosphor to accelerate the electrons across the tube. Positively charged focusing electrodes are used in the tube to minify the large beam of electrons down to the 1” output phosphor size. In the process the beam is also inverted therefore the image is reversed. The accelerated electrons will cause the light output from the output phosphor to be greater than the light output from the initial input phosphor. A closed circuit television chain is used to view the light output (image). Figure 6 shows a schematic representation of the x-ray transmission detection by the II.

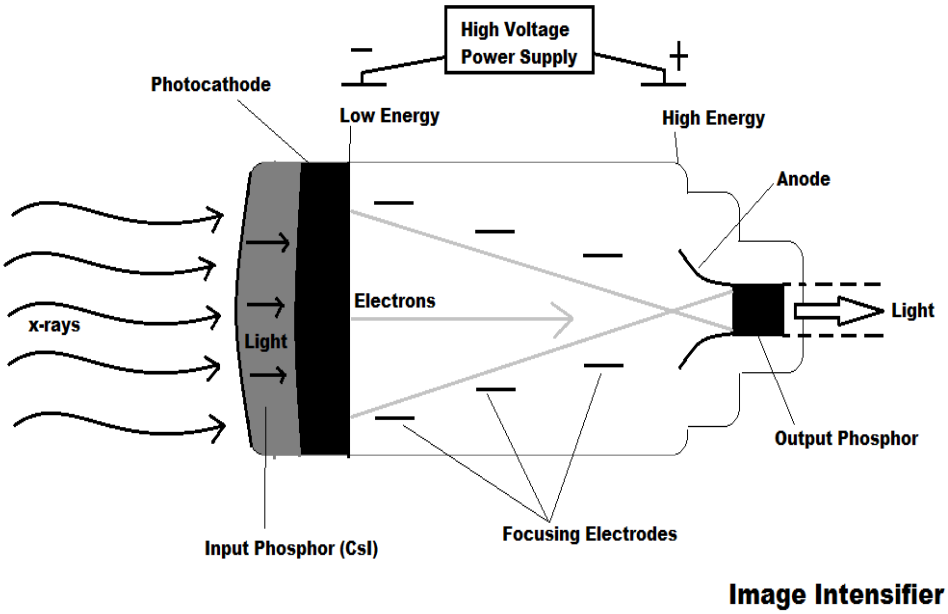

Figure 6. Diagram of the inner functions of an Image Intensifier. ***(Adapted from Huda, 2010)***[22]

The minification gain of an II is related to the input area divided by the output area, and the brightness gain is found by multiplying the minification gain by the flux gain. When fluoroscopy was first introduced the light output for the image was so poor that Radiologists would need to adjust their eyes in a dark room prior to imaging, but the II has greatly increased the image brightness so that images can be easily viewed on TV monitors now.

There are however four types of image artifact that are inherently present in fluoroscopy due to the II. The first is an optic distortion that occurs from the transfer of information through a curved input to a display on a flat output. This is known as Vignetting and is easily seen in the images as pixel value loss in the outer pixels of the image (ie. image

brightness decreases in the peripheral image). The second is due to the electric fields not being able to control the motion of the electrons as well in the peripheral as they do in the center of the output phosphor. This creates a wave like distortion in the peripheral image and is referred to as the pincushion effect.[23] S distortion is caused by nearby magnetic fields that effect how the electrons strike the output phosphor, and can create an S wave in the image. Finally the fourth type of artifact is veiling glare. This image degredation happens when light photons are scattered and reflected within the imaging system to create an abnormally bright area or glare in the image. Examples of each of these categories of artifact are illustrated in Figure 7.

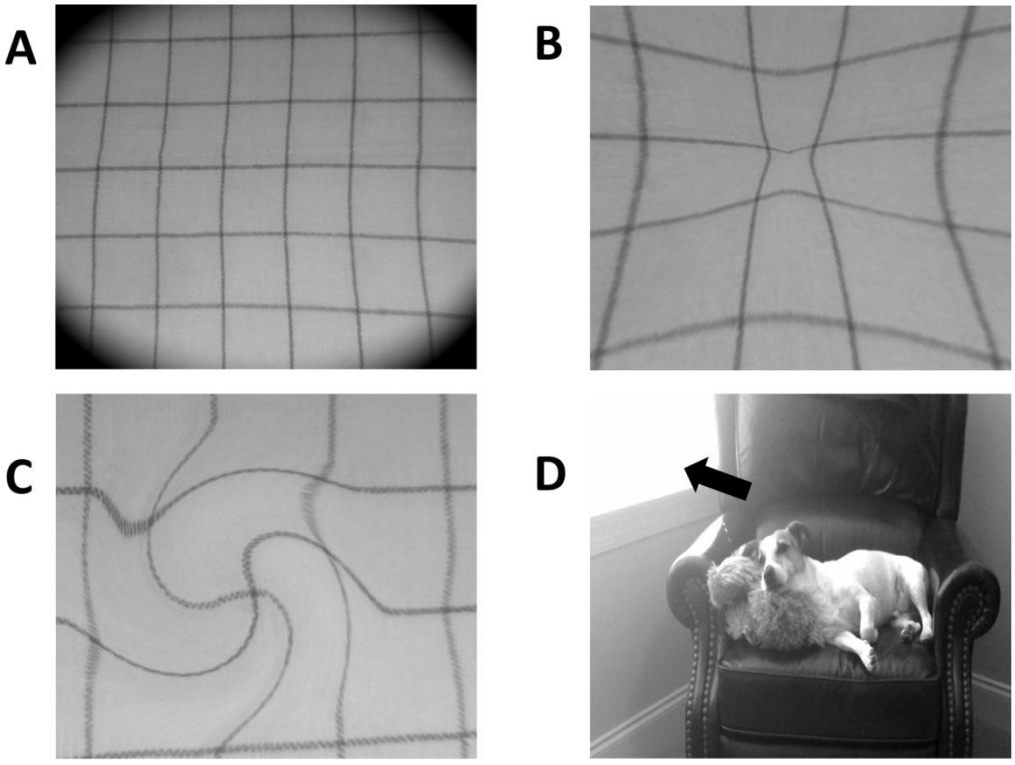

Figure 7. Four categories of image artifacts caused by the II: (A) Vignetting, (B) Pincushion Effect, (C) S Distortion, and (D) Veiling Glare.

2.3.2.2. Digital Subtraction Angiography

Digital Subtraction Angiography (DSA) can be accomplished using several different methods, but the most common method is to use a type of mask subtraction. A pre-contrast image is digitally recorded under fluoroscopy, and then a series of images are taken sequentially as a high atomic number x-ray contrast such as iodine is injected either intravenously or intra-arterially at a typical rate of one exposure per second.[23] During the image processing phase the pre-contrast image is electronically subtracted, or filtered, from each of the sequential images resulting in an enhanced view of the filling and draining of the particular arteries or veins of interest. Figure 8 shows a typical DSA image series for the brain.

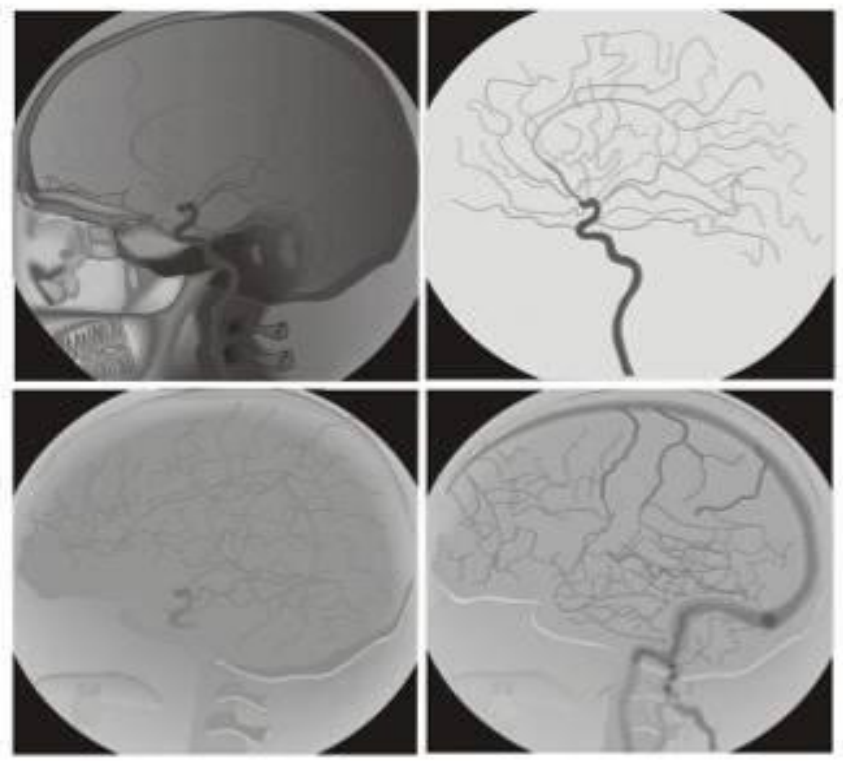

Figure 8. DSA image series with the top left image as the initial pre-contrast image. Over time the image will begin to look more like the original as the contrast washes out. ***(Courtesy of B. Jacobson et al., 2006)***[24]

2.3.3. Radiation Dose Monitoring

2.3.3.1. Kerma Area Product

The Kerma Area Product (KAP) previously referred to as the Dose Area Product (DAP) is the integral of the air kerma distributed across the entire x-ray beam, or the measurement of the total radiation incident on a patient during a given procedure.[25-27] KAP is the average x-ray beam intensity (air kerma) multiplied by the cross sectional area of the beam, and is generally measured in some form of Gy-cm^2.[25, 27] The measurement does not include the backscatter produced by the patient, and does include any field non-uniformities such as the anode-heel effect.[28] The KAP is also independent of the measurement location due to the inverse variations of the air kerma and cross sectional area. As the distance increases from the x-ray tube the air kerma decreases in accordance with the inverse square law, but the cross sectional area increases with distance from the x-ray tube such that the changes are opposite and equal.[27-28]

KAP can be measured using a conventional ionization chamber placed between the final collimator shutters and the patient, or measured in real time using an algorithm that accounts for the x-ray generator settings and collimation data.[28] KAP can also be used to estimate the patient's skin dose during a procedure. However the KAP does not provide any information on the spatial distribution of the entrance beam, so if the beam is moved throughout the procedure the KAP will provide an overestimation of the entrance skin dose.[26-28] The actual energy absorbed from the x-ray beam by the patient will be dependent on the patient characteristics (weight, body habitus, etc), so the KAP should not be confused with the actual absorbed dose to the skin or patient.[27]

2.3.3.2. Interventional Reference Point

The Interventional Reference Point (IRP) dose was defined by the International Electrotechnical Commission (IEC) standard 60601-2-43 to be at a location point representative of the patient's skin.[26, 28] IRP is the cumulative air kerma measured at a point along the central line of the x-ray beam 15 cm from the isocenter in the direction of the focal spot.[25-26, 28] It is the approximate radiation dose to the skin, but does not take into account the air to tissue dose conversion, backscatter, or actual location of the patient.[25, 28] Depending on the positional height of the table, patient size and x-ray beam placement the IRP may be located inside or outside the patient, and may or may not be at the skin entrance.[25, 28] The Food and Drug Administration (FDA) mandates that all fluoroscopy units introduced in the US market after March 2004 have the capability to measure the IRP, and the allowable uncertainty in the IRP measurement can be ±35%.[25, 28] The FDA also provides guidance on the location of the IRP in fluoroscopy units with non-isocentric geometries.[25]

2.3.3.3. Effective Dose

Effective dose (E) is the unit of radiation dose measurement that normalizes the incident body region exposure to that expected for a uniform whole body exposure.[29] The effective dose allows risk estimation to be made and comparison of different radiation exposures between medical modalities. It is defined as:

$$E = \sum_i w_i \cdot H_i$$

where the effective dose is the sum of the tissue weighting factor for tissue *I and* H_i is the equivalent dose to tissue *i.* The tissue weighting factors shown in Table 2 are defined by the International Commission for

Radiological Protection (ICRP) Publication 103 and represent the relative individual organ radiosensitivity.

Table 2. ICRP Publication 103 Tissue Weighting Factors (w_i).[30]

Tissue	w_i
Bone-marrow (red), breast, colon, lung, stomach, remainder tissues	0.12
Gonads	0.08
Bladder, esophagus, liver, thyroid	0.04
Bone surface, brain, salivary glands, skin	0.01

The equivalent dose (H_i) is the absorbed dose to a particular organ or tissue multiplied by the Relative Biological Effectiveness (RBE) factor:

$$H_i = D \cdot w_r$$

where D is the absorbed dose in units of Gray (Gy) measuring the amount of incident radiation per unit mass of a tissue (1 Gy = 1 J/kg), and w_r refers to the RBE. The RBE is a factor that accounts for the various levels of tissue damage each type of radiation is capable of (ie. 1 Gy of alpha particles will have a different biological effect than 1 Gy of x-rays). RBE factors are dependent on the radiation quality (Linear Energy Transfer, LET), radiation dose, number of dose fractions if the dose is fractionated, dose rate, and the target biologic system.[31] Table 3 lists the ICRP 103 recommended RBE factors.

Table 3. Relative Biological Effectiveness (RBE) Factors.[30]

Radiation	w_r
Alpha particles, fission fragments and heavy nuclei	20
Protons (energies > 2 MeV)	2.0
Photons (all energies)	1.0
Electrons (all energies)	1.0
Neutrons (energy dependent)	2.5 – 20

2.4. Regulations

2.4.1. Imaging Equipment

On September 30, 1994 a recommendation from the US Food and Drug Administration (FDA) stated that "information permitting estimation of the absorbed dose to the skin be recorded in the patient's medical record."[32] The concept of a cumulative dose (CD) was introduced in 2000 by the International Electrotechnical Commission (IEC), which is a measurement of the air kerma value at the Interventional Reference Point (IRP). The IRP is located along the central ray at 15 cm from the isocenter in the direction of the x-ray tube, and can be used to estimate the total radiation dose to the skin if it was summed over the entire body.[25] As of March 2004 all new fluoroscopic units are required by the FDA to be compliant with the IEC 60601-2-43 standard. The maximum allowable uncertainty according to the FDA for the IRP dose is ± 35%.[25]

The FDA also mandates that each fluoroscopy system have a 5 minute audible alarm that sounds after 5 minutes of fluoroscopic imaging. At 30 cm from the II for any source to image distance (SID) in the normal

imaging modes the unit may not exceed 10 R min^{-1} and in the high resolution modes the unit may not exceed 20 R min^{-1} to be FDA compliant.[28]

2.4.2 Radiology Staff

The radiology staff involved in IR procedures are considered occupational radiation workers, so they are regulated by 10CFR20 Subpart C. Table 4 outlines the rules and regulations for annual radiation doses.

Table 4. 10CFR20.1201 Occupational Dose Limits.[33]

Radiation Dose Target	Annual Limit (Sv)
Total Effective Dose Equivalent (TEDE)	0.05
Sum of Deep Dose Equivalent (DDE) & Committed Dose Equivalent (CDE) to any individual organ	0.5
Lens of the eye	15
Shallow Dose Equivalent to the skin of the whole body or the extremities	50

In accordance with ALARA all staff present in the IR suite during a procedure are required by the institution's radiation safety plan to wear aprons equivalent to 0.25-0.5 mm of lead and thyroid shields of 0.35-0.5 mm lead to reduce their exposures. The personal dosimetry badges (usually Thermoluminescent detectors) are worn on the outside of the lead apron for accurate dose measurements as shown in Figure 9.

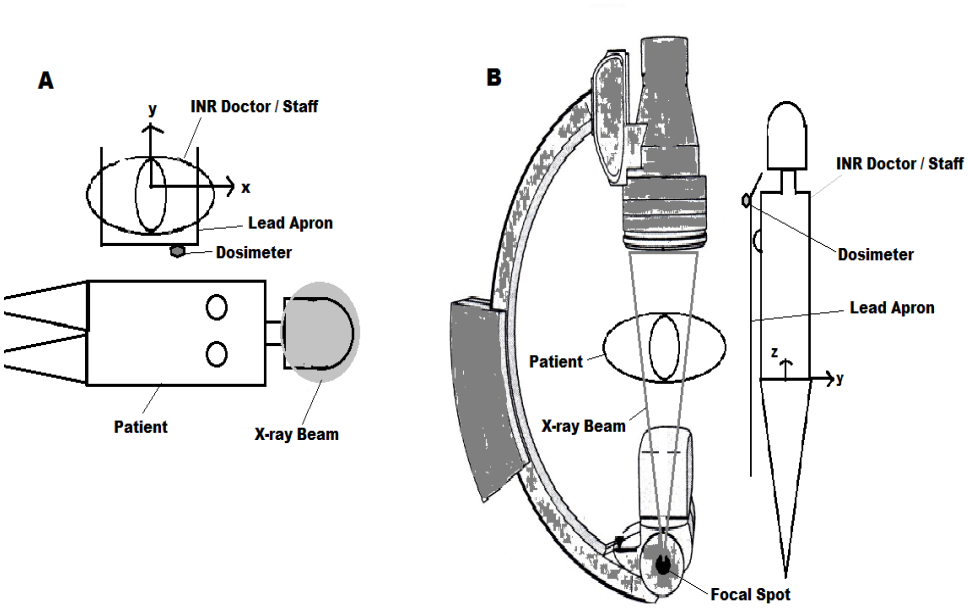

Figure 9. Diagram of a patient and IR staff member: (A) Arial view looking down on the patient, the grey circle is the x-ray beam; (B) Side view showing the x-ray tube focal spot and x-ray beam direction. ***(Adapted from T. Siiskonen et al., 2008)***[34]

2.4.3 Patient

The American College of Radiology releases practice guidelines for various types of radiology modalities and procedures. In their 2009 IR guideline for reporting and archiving one particular section outlines the archiving of patient radiation dose data: "if technically possible, all radiation dose data recorded by the fluoroscopy unit… should be transferred and archived with the images from the procedure… archiving of radiation dose data is of particular importance if the procedure is likely to be repeated or if the patient has received a clinically important radiation dose."[35] There are no current regulations for patient radiation doses, so what would be considered a "clinically important radiation dose" is left up to each individual institution to decide. At MUSC the current PACs system will not accept the radiation dose data from the fluoroscopy units. Hence the issue

of deciding which dose information is worth recording and where it should be recorded since it cannot be stored with the images.

Currently there are no federal regulatory requirements for recording or reporting IR patient radiation dose data.[25, 35-36] However, recently the federally recognized Joint Commission who certifies and accredits US hospitals has recognized radiation overdose as a Reviewable Sentinel Event. A radiation overdose is defined as “prolonged fluoroscopy with cumulative dose >1500 rads to a single field or any delivery of the radiotherapy to the wrong region or >25% above the planned dose.”[37]

2.5. Patient Risk

2.5.1. Non-stochastic Risk

Patient risk from radiation doses received during INR procedures can be divided into two categories: non-stochastic (deterministic effects) and stochastic risk (cancer risk). The most concerning deterministic effects in INR are erythema, cataracts, and epilation. The threshold doses and various deterministic effects are summarize in Table 5.

Table 5. Deterministic skin effects from single acute skin exposures. ***(Adapted from S. Balter et al, 2010)***[38]

Single Site Acute Dose Range (Gy)	Approximate time to onset of effects			
	Prompt	Early	Midterm	Long Term
2-5	Transient erythema	Epilation	Recovery from hair loss	No observable results expected
5-10	Transient erythema	Erythema, epilation	Recovery; at high doses prolonged erythema and permanent epilation.	Recovery likely except at higher doses, dermal atrophy or induration
10-15	Transient erythema	Erythema, epilation; possibility of dry or moist desquamation (likely recoverable)	Prolonged erythema; permanent epilation.	Telangiectasia; dermal atrophy or induration; skin likely to be weak
>15	Transient erythema; edema and acute ulceration; long term surgical intervention maybe required	Erythema, epilation; moist desquamation	Dermal atrophy; secondary ulceration, and at higher doses dermal necrosis; surgical intervention likely required	Telangiectasia; dermal atrophy or induration; possible late skin breakdown; wound might be persistent and progress into deeper lesions; surgical intervention required.

Cataracts are defined as an opacity in the normally clear lens of the eye. For a single exposure to the lens of the eye to produce a progressive cataract an absorbed threshold dose of 2 Gy is required. For fractionated doses spread over a three week to three month period this minimum threshold dose increases to 4 Gy. Cataracts typically have an 8 year latency period for absorbed doses of 2.5 – 6.5 Gy.[31] It has been proposed that eye doses can be derived from patient thyroid dose as follows:

$$\textbf{Eye Dose} = 0.75 \times \textbf{Thyroid Dose}$$

where the eye doses are the doses to the Radiologist's eyes.[39]

2.5.2. Stochastic Risk

The Biologic Effects of Ionizing Radiation (BEIR) VII reports published in 2005 by the National Academy of Science focuses on radiation health effects of low levels of low-LET ionizing radiation such as x-rays and gamma rays. These reports use the epidemiological data gathered by the atomic bomb survivors of Hiroshima and Nagasaki as well as data gathered from a few medical cohorts. This report provides age and gender specific cancer risk and mortality data. The most radiosensitive organs at risk for cancer induction are thyroid, stomach, colon, liver, lung, female breast, uterus, ovaries, prostate, and bladder. Of these organs the only one excluded from the data for risk of cancer mortality is the thyroid. In INR imaging the predominant focus is in the head and neck region, so the target organ of concern for cancer induction is the thyroid gland.[40]

3. MATERIALS AND METHODS

3.1. Characterization of Radiation Beam Geometry

Patient radiation dose summaries were collected for 75 INR procedures at MUSC completed during February 2010. Of those 75 procedures 7 were automatically excluded from the study on the basis of age. The remaining 63 patients were all adult patients over the age of 18. The exam protocol reports are accessible through the Siemens Axiom Artis BA acquisition and processing software at the completion of each study. The patient age, sex and exam type were the only non-radiation dose information provided with the reports.

An example of an exam protocol report is shown in Figure 10. These reports provide the following information by line:

Line 1:
- Scene Number
- Acquisition Mode
- Acquisition Program
- Scene Duration
- Maximum Frame Rate
- Date and Time of Acquisition

Line 2:
- Acquisition Plane (A or B)
- X-ray Tube Voltage (kV)
- X-ray Tube Current (mA)
- Exposure Time (ms)
- X-ray Tube Focus
- Additional filtration (mm of Cu)
- II Image Zoom Level
- DAP (μGy m^2)
- IRP Dose (mGy)
- Projection Data (ie. LAO, RAO, CRAN, or CAUD)
- Total Number of Acquisitions per scene

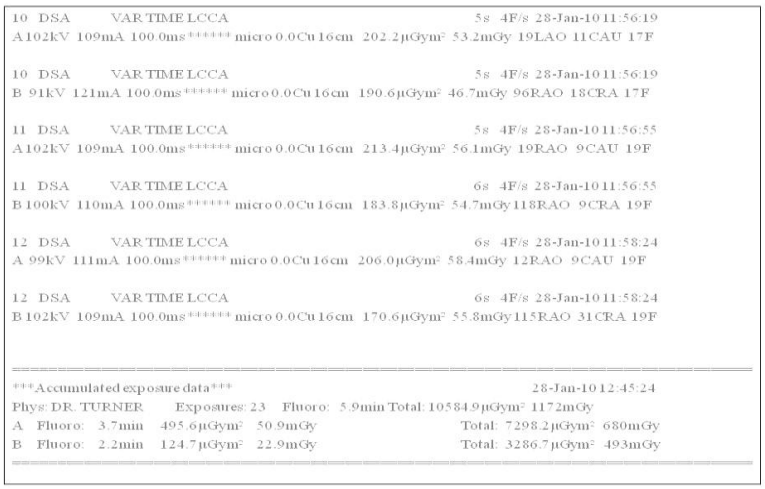

Figure 10. Example of the Siemen's Axiom Artis BA patient exam protocol radiation dose information data collected on a February 2010 adult patient.

At the end of each report if the patient's file is closed out properly before the next patient procedure commences a fluoroscopy summary report is included with radiation dose information for each plane consisting of the DAP, IRP dose, and fluoroscopy time. 29 of the 63 adult patient's reviewed had fluoroscopy summary reports included in their exam protocol reports. This data was used to characterize the radiation geometry, beam profile, for the typical DSA and fluoroscopy profiles used in INR procedures.

The image projection data was also profiled with the radiation beam geometry, since the organ dose to the thyroid and lens of the eye will be somewhat dependent on the entrance and exit area of the x-ray beam during the procedure. Figure 11 illustrates the optional image projections the Axiom Artis BA biplane is capable of.

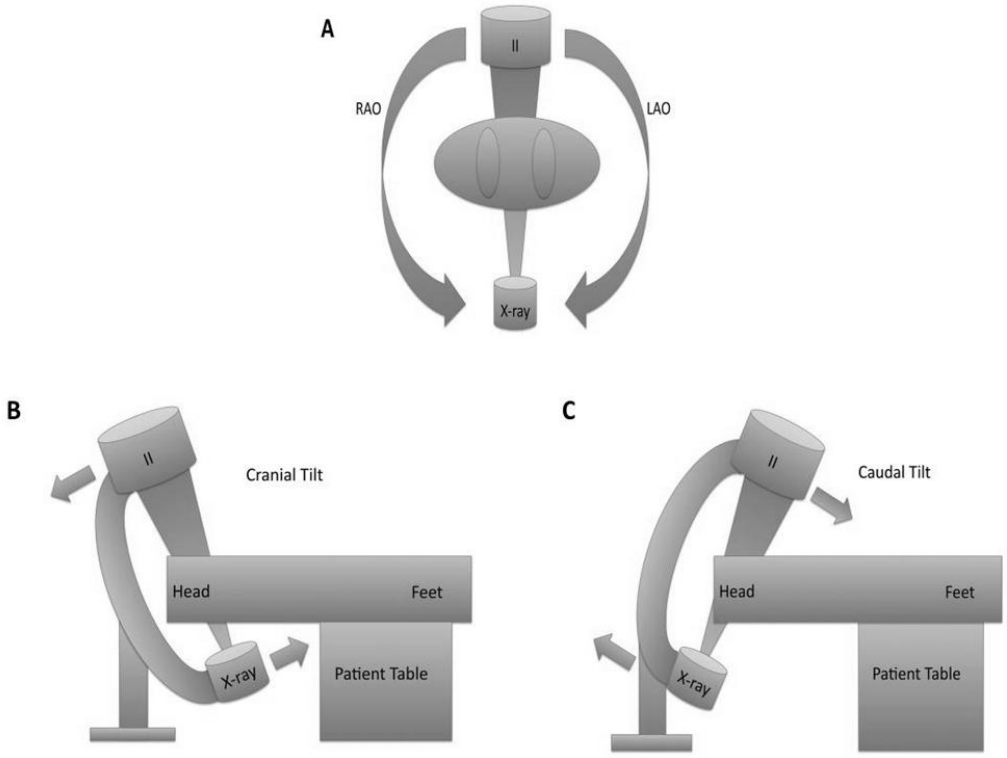

Figure 11. Image projections (A) RAO and LAO projections viewed from the patients feet towards the head, (B) Crainal tilt (II tilted towards the head), and (C) Caudal tilt (II tilted towards the pelvis).

3.2. Effective and Organ Dose Conversion

PCXMC (version 2.0) is a software package that can be used for calculating absorbed organ doses and the corresponding effective dose to a patient undergoing a diagnostic x-ray examination.[41] The program calculates the effective dose with the tissue weighting factors from the ICRP 2007 Publication 103 recommendations.[30] The anatomical data are based on the slightly modified model of the mathematical hermaphrodite 1987 Cristy and Eckerman phantom.[42] In this study, a standard size adult phantom, which weighed 73.2 kg, with a height of 178.6 cm was used in the simulations.

PCXMC allows the user to define the patient irradiation geometry, where the isocenter is always located in the geometric center of the ellipse that defines the patient cross-section. The user can define the image area both in vertical and horizontal directions, the focus to detector distance (FDD), as well as the patient-exit to detector distance. To compute doses, the reader has to define the key factors that influence the x-ray beam quality. A tungsten target is used, and up to two added x-ray beam filters can be specified by the user. Default values commonly utilized are Aluminum (Z = 13) and Copper (Z = 29), with the thickness of each definable during simulations. Definition of these parameters permits the simulation of the irradiation geometries used in INR. The numerical parameters are outline in appendix B for planes A and B.

There are three ways of normalizing a given computation: (a) entrance skin dose (mGy); (b) KAP (or DAP) in mGy cm^2, where the air kerma is determined “free in air”; and (c) by using a constant x-ray tube output as specified by the x-ray tube current exposure time product (mAs). All the calculations performed in this study were normalized to KAP to establish effective dose as a function of the KAP at multiple x-ray tube voltages. The total effective dose (E) (mSv) can be calculated by summing the effective dose for each body region and each plane in that body region as follows:

$$E_{(mSv)} = \sum E_H + E_N + E_C + E_{A/P}$$

where E is the effective dose (mSv) as a function of the sum of the total effective dose calculated from the KAP by plane, body region, and x-ray tube voltage. E_H is the effective dose in the head region, E_N is the effective dose in the neck region, E_C is the effective dose in the chest region, and

$E_{A/P}$ is the effective dose from the abdomen and pelvis regions. The organ dose for the thyroid can be generated in an identical manor using the conversion factor specific to thyroid dose (D_T) (mGy) as follows:

$$D_{T(mGy)} = \sum D_{T(H)} + D_{T(N)} + D_{T(C)}$$

Since the two main venous access points are located in the arm and groin area some fluoroscopic imaging will be used to guide the catheters through the patient's trunk to the head and neck. This imaging will affect both the effective dose and thyroid organ dose, so it must be accounted for by the total KAP used in each plane for each body region. Figure 12 illustrates the body regions of the anthropomorphic mathematical phantom used in the simulations.

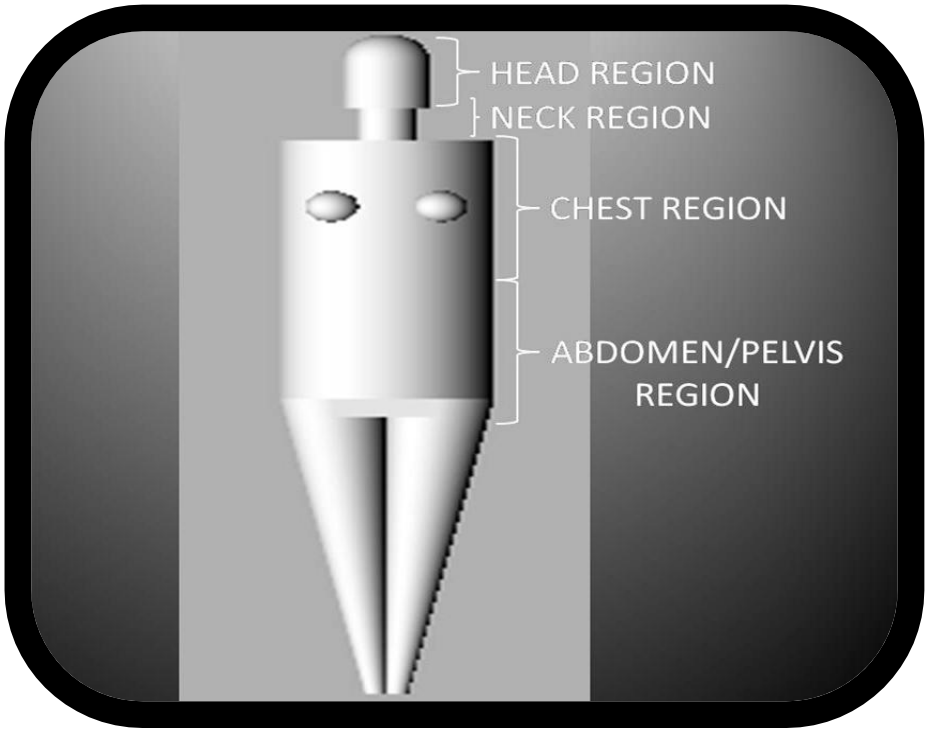

Figure 12. Body regions of the anthropomorphic phantom. ***(Adapted from PCXMC 2.0)***[43]

3.3. Stochastic Risk Conversion

The BEIR VII data was used to estimate the risk of thyroid cancer as a function of the age and sex specific data provided in the report. The data is arranged by the incidence of thyroid cancer per 100,000 individuals who each receive an absorbed dose of 100 mGy during a single exposure. The conversion of patient organ dose to risk is possible also taking into account patient specific criteria such as age and sex at the time of their INR procedure. Therefore if the thyroid organ dose is calculated an approximate risk of thyroid cancer incidence can be calculated specific to the patient's age and sex as a function of their procedure as follows:

$$R_P = \frac{Risk_{Age \cdot Sex}}{(100{,}000 cases)(100 mGy)} \times D_T$$

where R_p is a thyroid cancer incidence risk percentage specific to a patient's procedural thyroid dose (D_T) in mGy based on their individual risk as a function of age and sex based on the BEIR VII data.

4. RESULTS

4.1. Radiation Beam Geometry

Figures 12 and 13 are histograms of the x-ray tube voltages used during the DSA procedures for all therapeutic and diagnostic procedures. The majority of x-ray tube voltages used with a 0.1 mm copper (Cu) filtration were under 80 kV (Figure 13), but when no filtration was used the typical x-ray tube voltage ranged between 95 kV to 105 kV in Plane A and were more varied in Plane B with the two most used voltages at 72 kV and 102 kV (Figure 12).

The highest voltage used was 125 kV with no filtration and the overall voltages are generally lower when filtration was used. There were 913 runs with no filtration and 87 runs with 0.1 mm Cu filtration in Plane A alone. In Plane B there were 636 runs with no filtration and 239 runs with 0.1 mm Cu. Runs with no filtration used were 91.3% in Plane A and 72.7% in Plane B, so the no filtration runs in both planes totaled 82.6% of all runs.

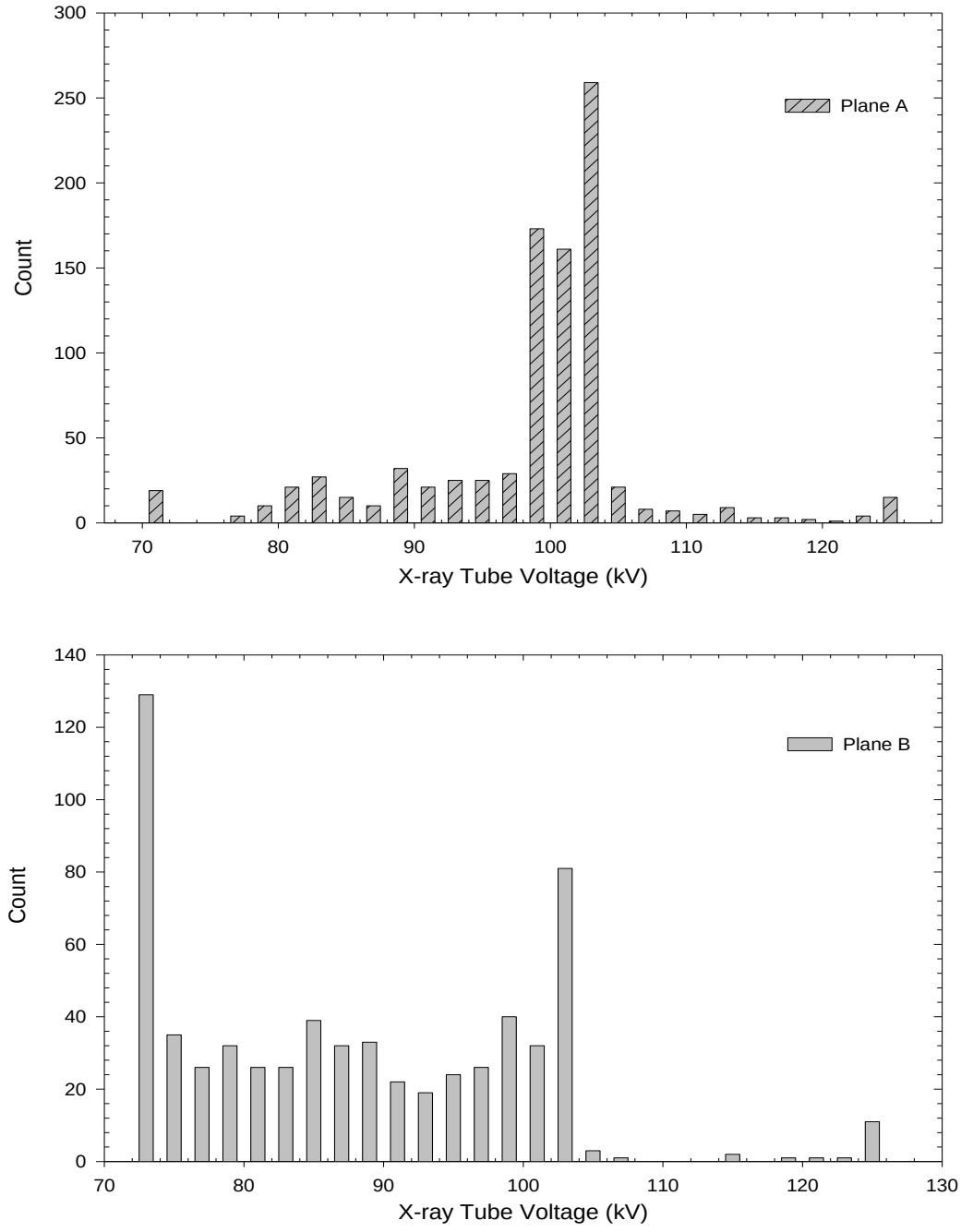

Figure 13. Histogram of x-ray tube voltages for two radiation planes used with no filtration in the beam for all INR procedures.

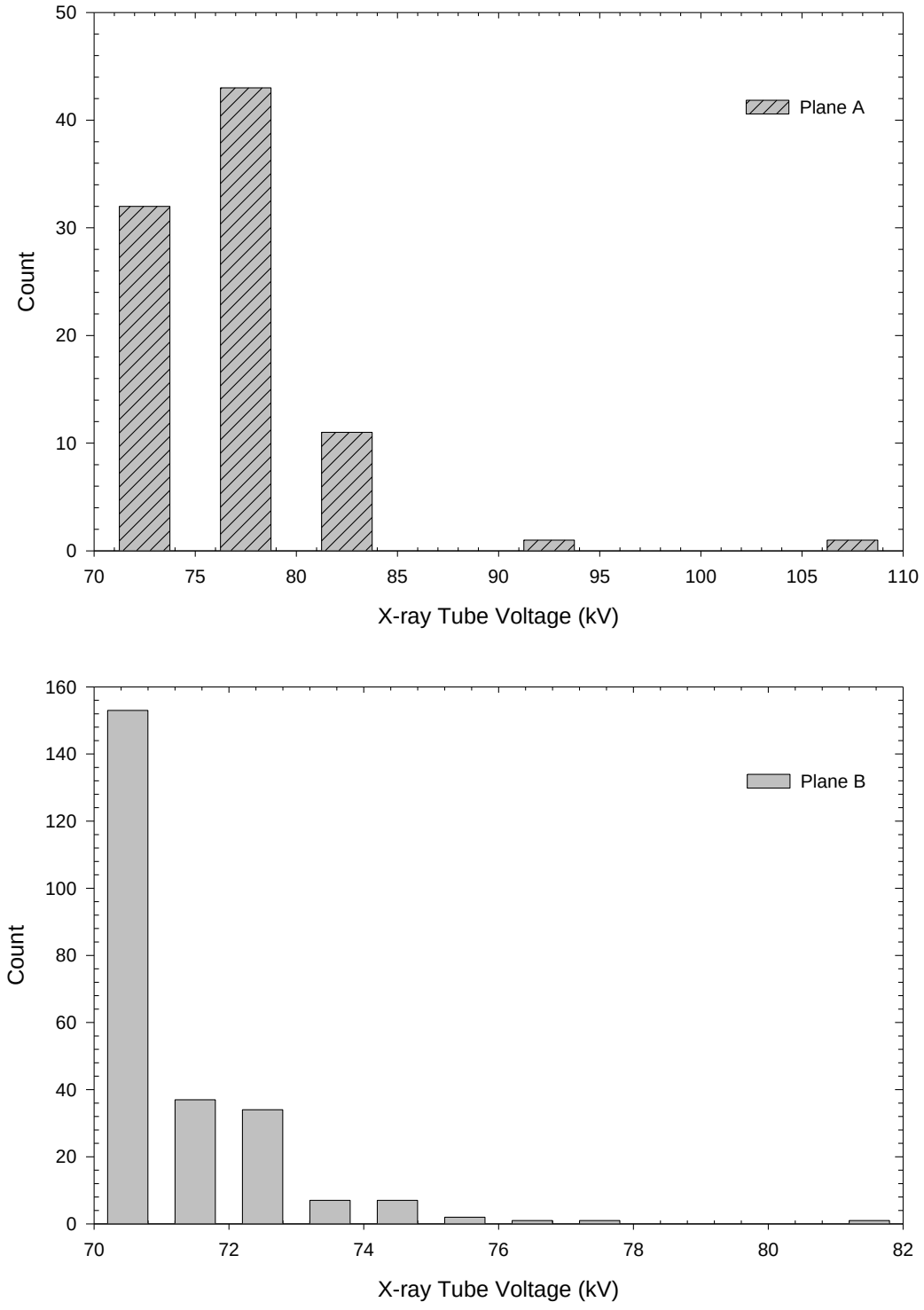

Figure 14. Histogram of x-ray tube voltages for two radiation planes used with 0.1 mm Cu filtration in the beam for all INR procedures.

The II diameter corresponds to the image size, and Figure 14 shows histograms of the II diameters used in both planes during all DSA procedures. Plane A has a greater range of II diameter sizes (cm) than plane B by a factor of ~1.8. The most used II diameters of Plane A are 11 cm (12.6%), 16 cm (24.3%), and 32 cm (47.0%). The most used II diameter of Plane B is 25 cm (51.5%), which is approximately 2.6 times more often used than the next greatest II diameter of 20 cm (19.5%).

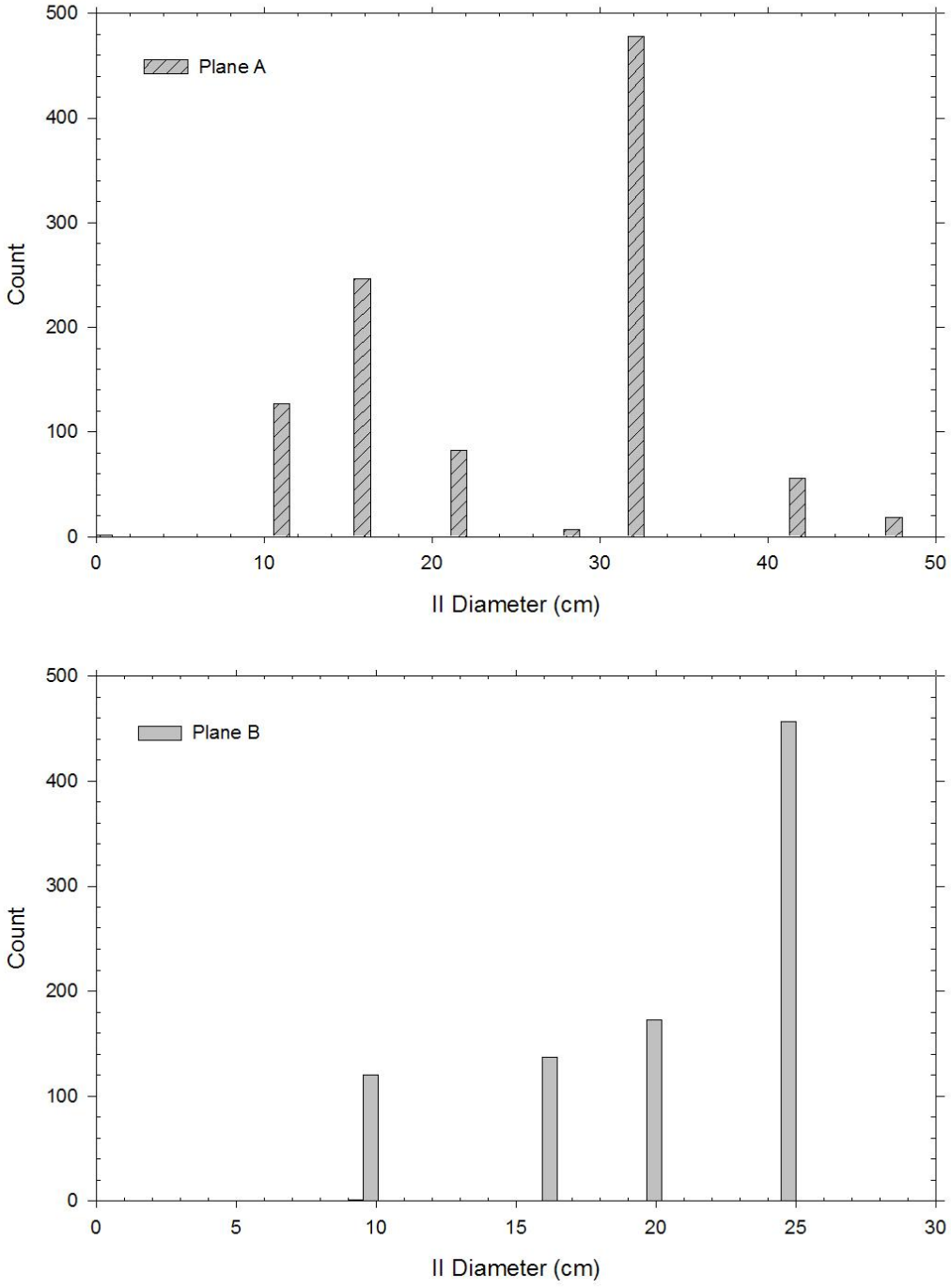

Figure 15. Histogram of II diameters used in two independent planes in the recorded during all INR procedures studied.

Figures 15 and 16 show the total time of each run in seconds and number of frames per run. A majority of the runs performed in Plane A and B were between 5 to 10 seconds. The majority of frames per run were between 15 to 30 frames for both planes. This is also indicative of the frame rate being constant throughout each DSA run (4 sec/frame). The total time for each procedure is variable dependent on the procedure and patient.

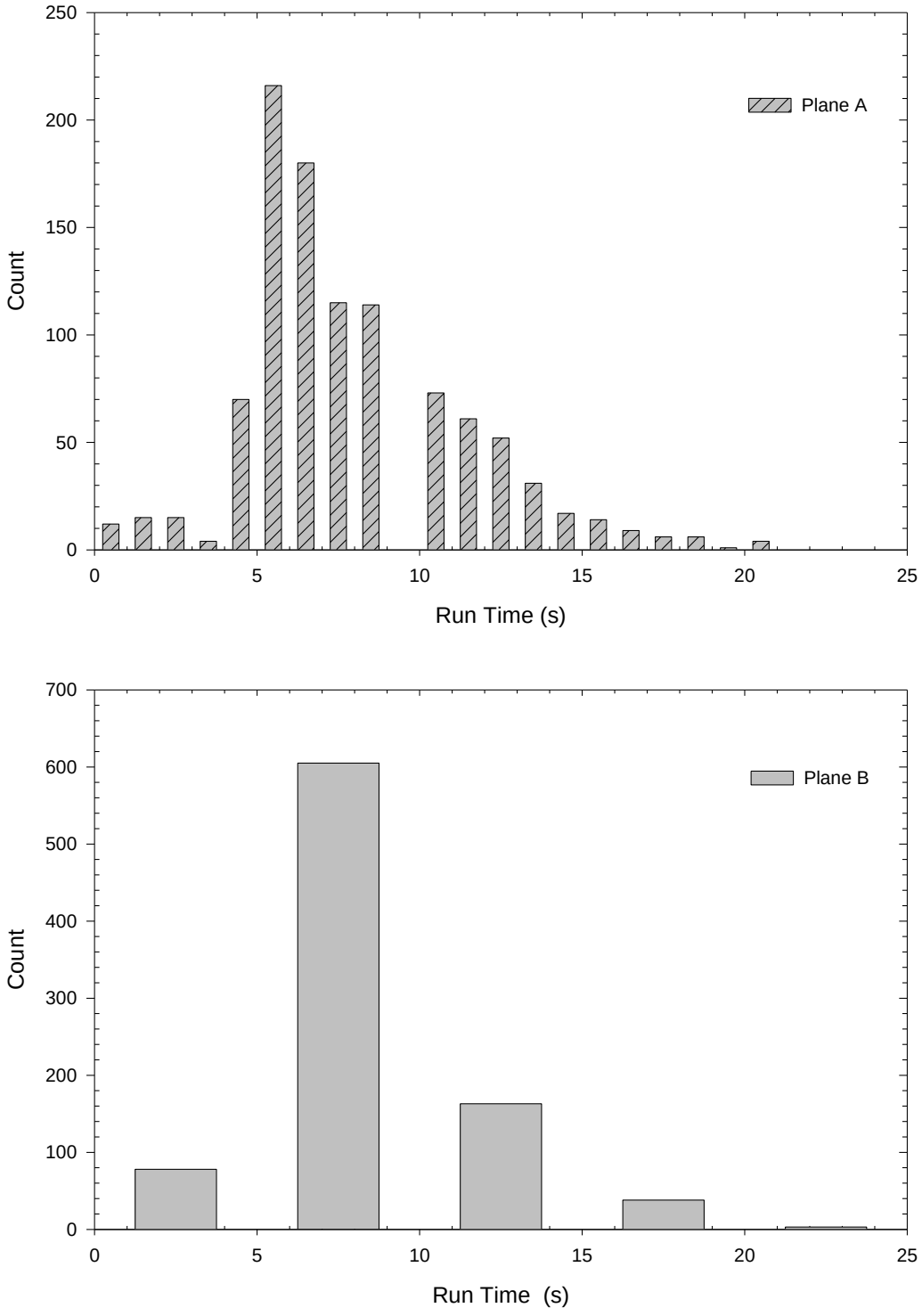

Figure 16. Histogram of overall run time for each set of DSA images with multiple frames acquired.

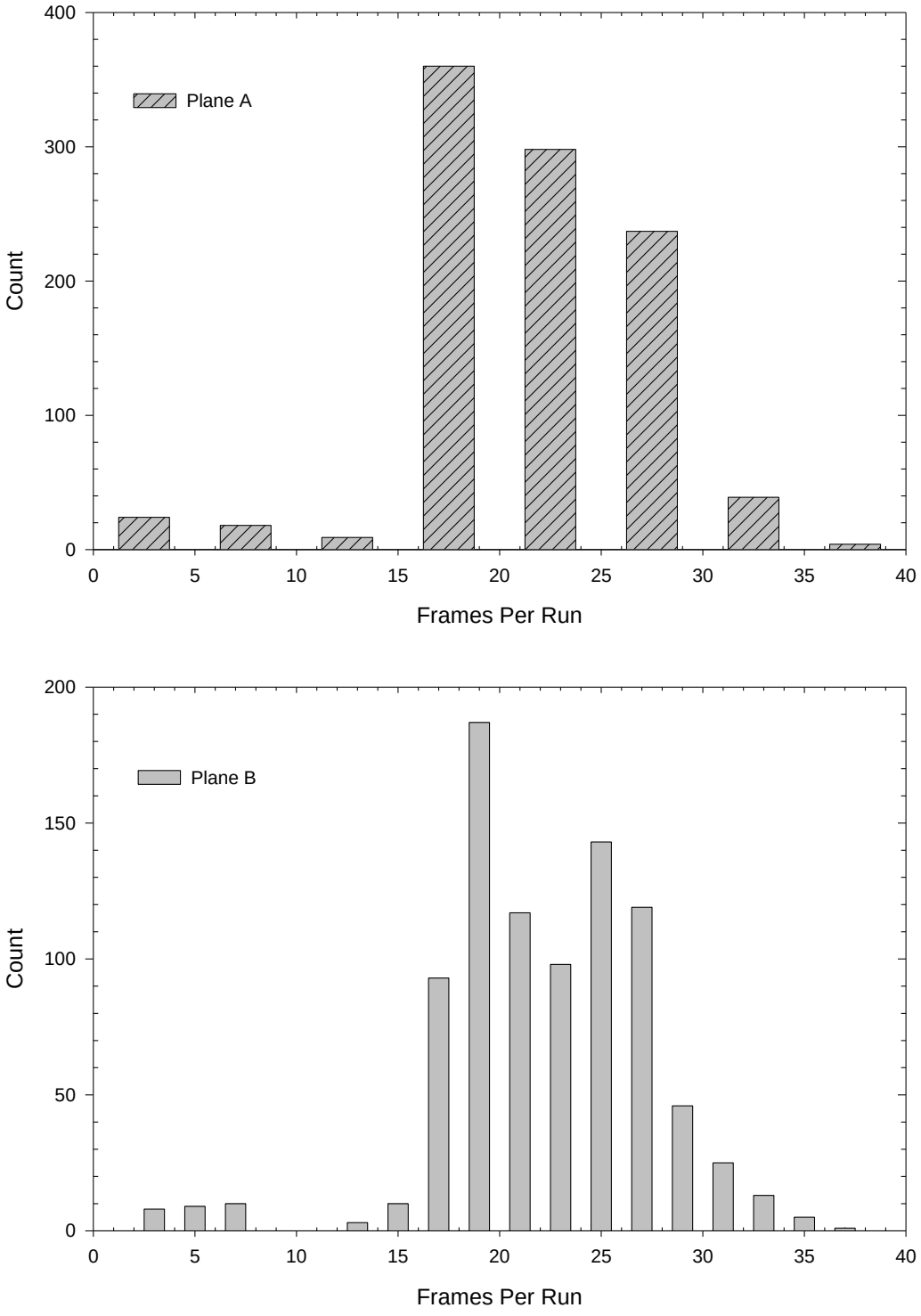

Figure 17. Histogram of the number of frames per each DSA imaging acquisition.

Figures 17 and 18 profile the image projection angles used in all DSA runs. Figure 17 shows a graphical representation of an anterior view of the patient as if looking down on the patient lying on the table from the II for Plane A, and a lateral view of the patient lying on the table from the point of view of the II in Plane B. Angles in degrees are recorded for the II in relation to patient for each DSA run. The dots on the graphs represent the degrees most used in these runs. It is of interest to note that although many angles are used most of these data points are centered along the central lines of the patient in the anteroposterior and lateral directions. Figure 18 shows two histograms for each plane showing the Right Anterior Oblique (RAO) / Left Anterior Oblique (LAO) angles and the Caudal / Cranial angles.

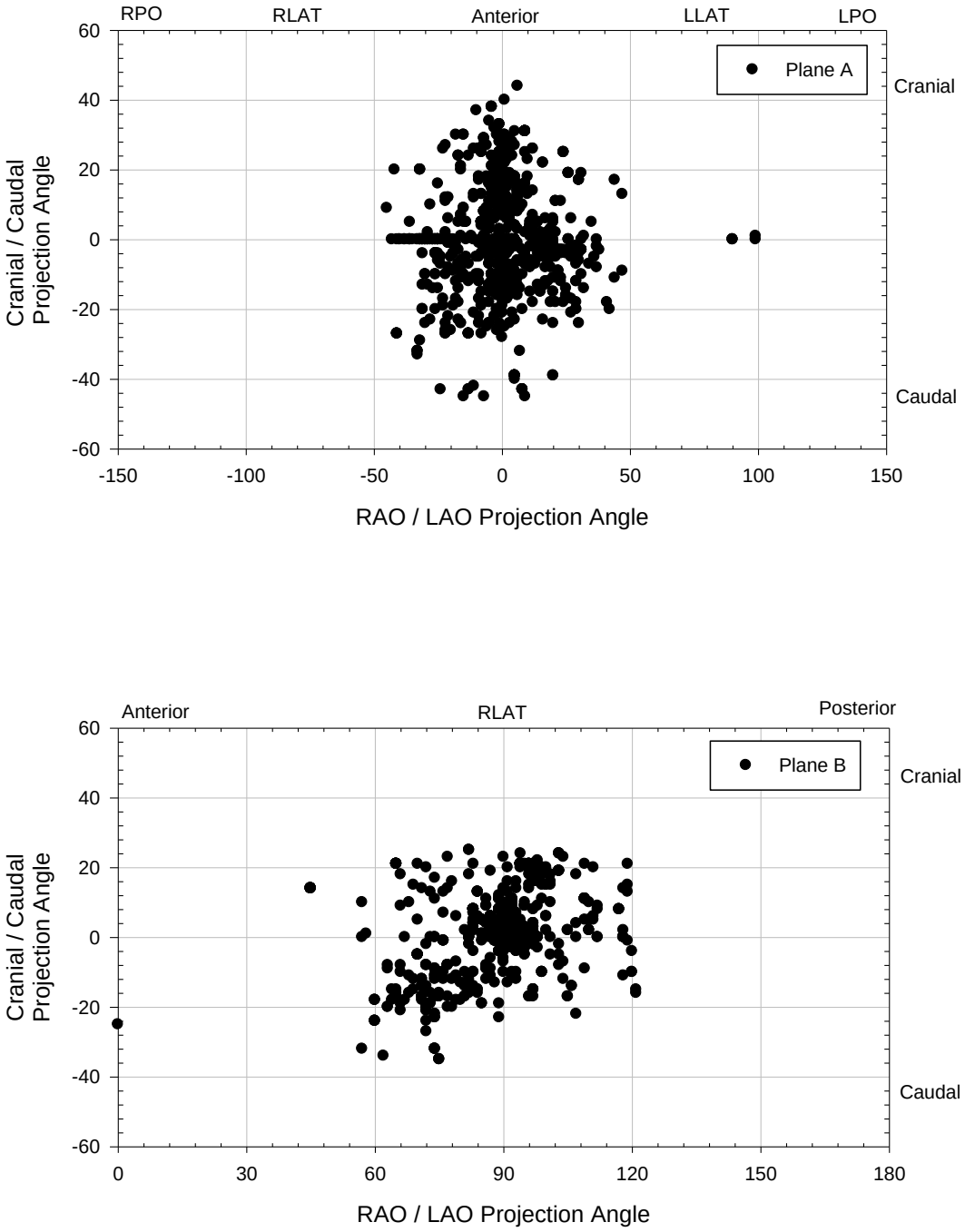

Figure 18. Representative projection imaging angles in planes A and B.

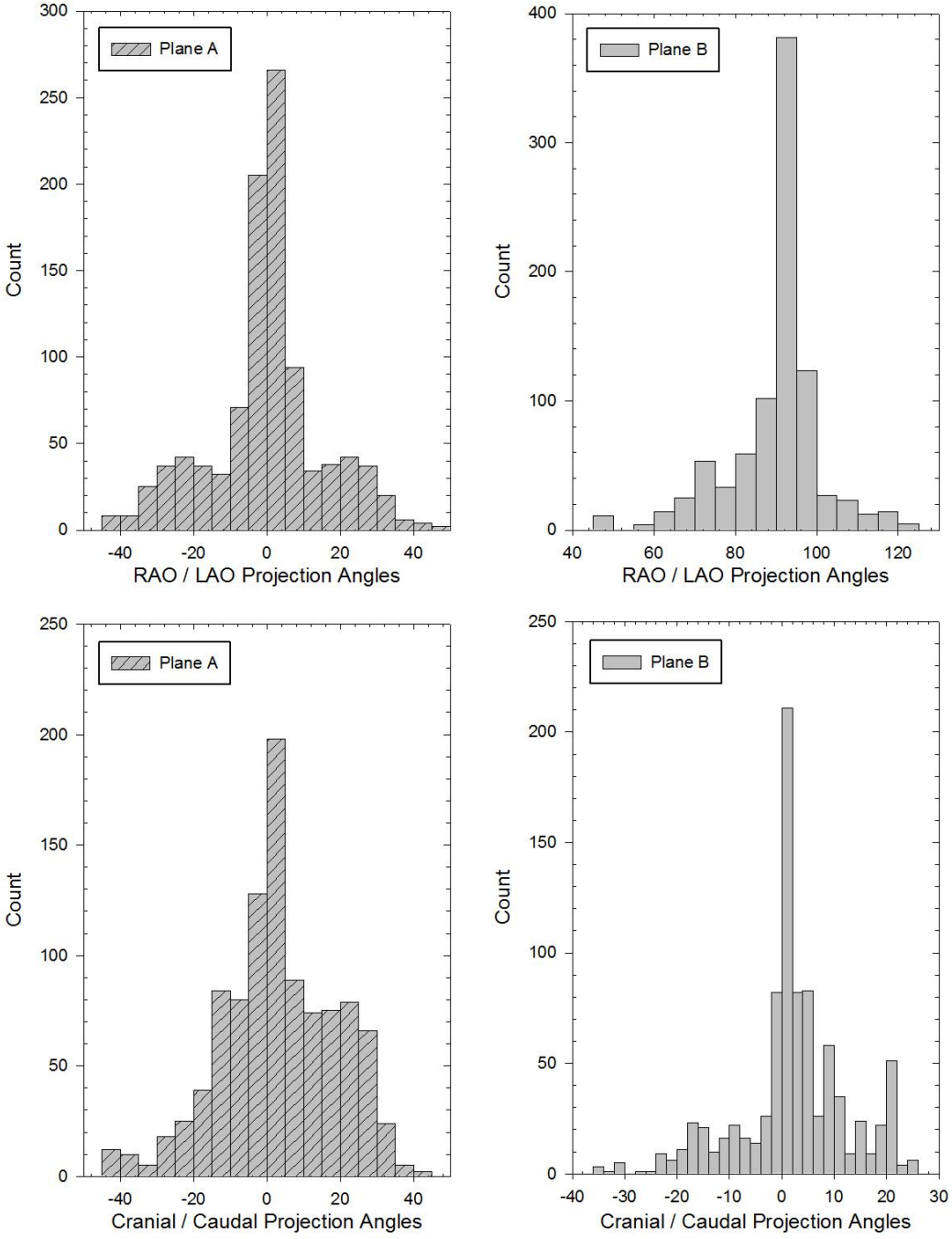

Figure 19. Histograms of image projection angles used in planes A and B during all INR procedures.

For all INR patients whose fluoroscopy radiation dose data was also recorded in the exam protocol summary a comparison of the radiation dose data from the DSA to the fluoroscopy runs are shown in Table 6 and 7. Table 6 shows the KAP divided by Plane for DSA and Fluoroscopy (F) runs. This table also gives a percentage value for the KAP for Plane A compared to the total between both planes. Table 7 shows the KAP divided by DSA and Fluoroscopy (F) runs, and gives a percentage for the KAP of the DSA runs compared with the total KAP of both the DSA and Fluoroscopy runs. In all but one case the DSA accounts for more than 53% of the total KAP, and > 63% of the total KAP in all cases is from Plane A.

Table 6. KAP (Gy-cm^2) comparison for DSA and fluoroscopy (F) divided by planes A and B with a percentage for the Plane A KAP.

	A (Gy-cm^2)			B (Gy-cm^2)			Plane
	DSA	F	Total	DSA	F	Total	A
	63.71	5.14	68.84	36.27	1.20	37.47	65%
	37.06	6.70	43.76	25.91	1.49	27.40	61%
	134.08	20.97	155.05	44.87	7.96	52.83	75%
	137.66	77.92	215.58	111.84	26.17	138.01	61%
	109.52	62.04	171.56	32.33	23.56	55.89	75%
	158.32	126.22	284.54	77.59	73.12	150.70	65%
	68.58	13.63	82.20	36.00	1.70	37.71	69%
	82.10	54.53	136.63	43.93	14.53	58.46	70%
	35.38	4.28	39.65	18.05	0.55	18.61	68%
	108.21	22.11	130.32	45.55	5.19	50.73	72%
	207.58	111.50	319.07	51.82	23.98	75.80	81%
	80.33	13.09	93.42	36.40	2.22	38.62	71%
	79.27	20.67	99.95	39.58	4.34	43.93	69%
	118.40	64.85	183.25	39.62	29.32	68.94	73%
	63.19	55.05	118.24	28.09	2.41	30.50	79%
	44.47	7.04	51.51	19.79	1.33	21.12	71%
	73.85	208.68	282.53	41.77	95.22	137.00	67%
	27.27	6.88	34.15	14.65	1.28	15.94	68%
	109.03	132.97	241.99	45.45	2.06	47.50	84%
	75.57	20.39	95.96	34.29	2.83	37.11	72%
	89.29	21.61	110.89	54.13	2.90	57.02	66%
	16.05	2.74	18.80	4.11	0.07	4.18	82%
	70.29	18.36	88.65	38.36	2.04	40.40	69%
	25.23	9.64	34.87	8.46	0.69	9.15	79%
	32.79	17.05	49.84	15.32	0.66	15.98	76%
	69.18	29.14	98.32	26.05	10.24	36.29	73%
	132.37	36.19	168.56	46.94	7.90	54.84	75%
	69.94	41.31	111.26	31.47	2.91	34.38	76%
	64.79	44.38	109.17	22.40	13.18	35.57	75%
	94.79	46.92	141.71	39.38	9.61	48.99	74%
Average	82.6	43.4	126.0	37.0	12.4	49.4	72%
(± 2σ)	(86.3)	(94.5)	(158.2)	(41.1)	(42.9)	(71.3)	(0.12)

Table 7. KAP (Gy-cm^2) comparison of DSA and Fluoroscopy (F) divided by planes A and B with a percentage for the DSA KAP.

	DSA (Gy-cm^2)			Fluoroscopy (Gy-cm^2)			DSA
	A	B	Total	A	B	Total	
	63.71	36.27	99.98	5.14	1.20	6.33	94%
	37.06	25.91	62.96	6.70	1.49	8.19	88%
	134.08	44.87	178.95	20.97	7.96	28.93	86%
	137.66	111.84	249.50	77.92	26.17	104.09	71%
	109.52	32.33	141.85	62.04	23.56	85.60	62%
	158.32	77.59	235.90	126.22	73.12	199.34	54%
	68.58	36.00	104.58	13.63	1.70	15.33	87%
	82.10	43.93	126.03	54.53	14.53	69.06	65%
	35.38	18.05	53.43	4.28	0.55	4.83	92%
	108.21	45.55	153.75	22.11	5.19	27.30	85%
	207.58	51.82	259.40	111.50	23.98	135.48	66%
	80.33	36.40	116.73	13.09	2.22	15.32	88%
	79.27	39.58	118.86	20.67	4.34	25.02	83%
	118.40	39.62	158.01	64.85	29.32	94.17	63%
	63.19	28.09	91.28	55.05	2.41	57.46	61%
	44.47	19.79	64.26	7.04	1.33	8.37	88%
	73.85	41.77	115.62	208.68	95.22	303.90	28%
	27.27	14.65	41.92	6.88	1.28	8.16	84%
	109.03	45.45	154.47	132.97	2.06	135.03	53%
	75.57	34.29	109.85	20.39	2.83	23.22	83%
	89.29	54.13	143.41	21.61	2.90	24.51	85%
	16.05	4.11	20.17	2.74	0.07	2.81	88%
	70.29	38.36	108.65	18.36	2.04	20.40	84%
	25.23	8.46	33.69	9.64	0.69	10.33	77%
	32.79	15.32	48.11	17.05	0.66	17.71	73%
	69.18	26.05	95.23	29.14	10.24	39.38	71%
	132.37	46.94	179.31	36.19	7.90	44.09	80%
	69.94	31.47	101.42	41.31	2.91	44.22	70%
	64.79	22.40	87.19	44.38	13.18	57.55	60%
	94.79	39.38	134.17	46.92	9.61	56.53	70%
Average	82.6	37.0	119.6	43.4	12.4	55.8	75%
(± 2σ)	(86.3)	(41.1)	(120.3)	(94.5)	(42.9)	(132.6)	(0.3)

4.2. Effective and Organ Dose Conversion

Figures 20 - 23 illustrates how the effective dose (E) changes with the KAP incident on the patient in each body region. Least squares fit linear regressions were fitted to each set of data, and an equation for calculating E is displayed on each figure. The sum of E_H, E_N, E_C, and $E_{A/P}$ for plane A and B will yield the total effective dose for the procedure for all DSA and fluoroscopy runs if the KAP is known for each body section. The coefficients for each body region equation are listed in Tables 9 - 11 directly following each figure.

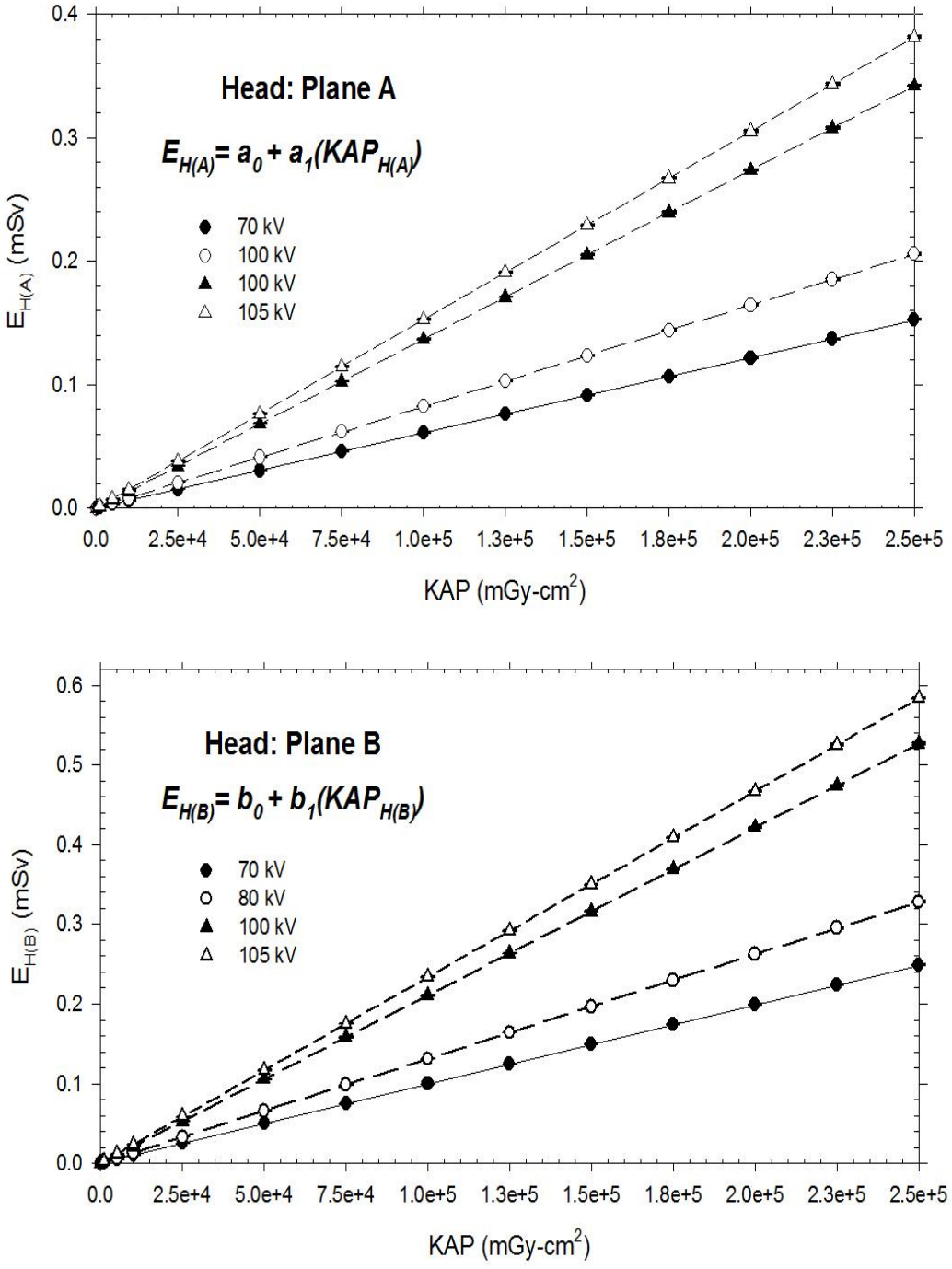

Figure 20. Effective Dose (E) in the head region for planes A and B as a function of the incident KAP for several x-ray tube voltages.

Table 8. Figure 20 equation coefficients for planes A (AP projection) and B (lateral projection) for multiple x-ray tube voltages (kV).

X-ray Tube Voltage (kV)	Plane A		Plane B	
	a_0	a_1	b_0	b_1
70	5.1E-8	6.1E-7	-5.2E-8	9.9E-7
80	-4.3E-8	8.2E-7	2.4E-8	1.3E-6
100	-5.5E-8	1.4E-6	-2.1E-7	2.1E-6
105	3.7E-8	1.5E-6	-1.1E-7	2.3E-6

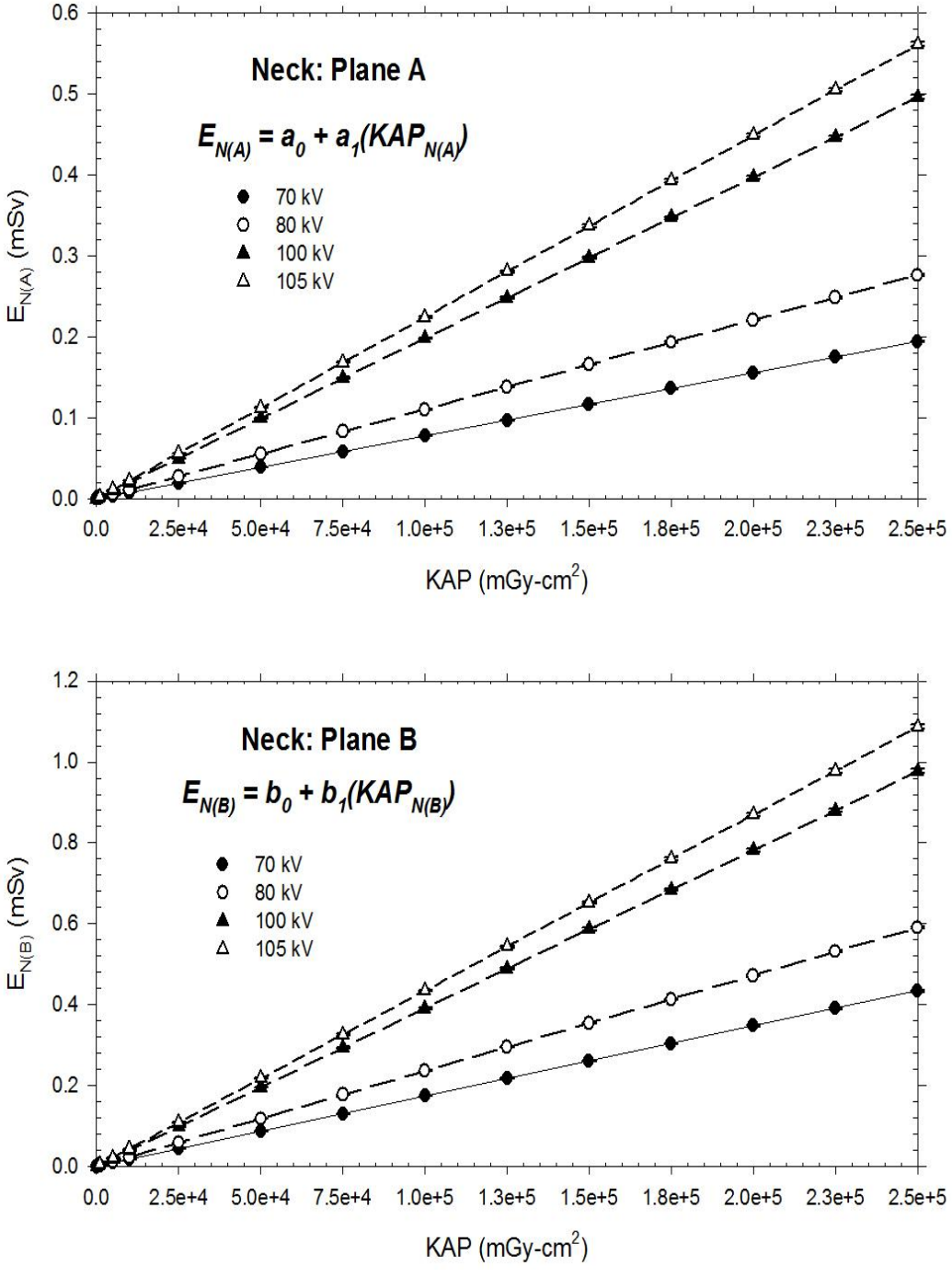

Figure 21. Effective Dose (E) in the neck region for planes A and B as a function of the incident KAP for several x-ray tube voltages.

Table 9. Figure 21 equation coefficients for planes A (AP projection) and B (lateral projection) for multiple x-ray tube voltages (kV).

X-ray Tube Voltage (kV)	Plane A		Plane B	
	a_0	a_1	b_0	b_1
70	1.3E-7	7.8E-7	9.5E-8	1.7E-6
80	2.3E-8	1.1E-6	-3.8E-8	2.4E-6
100	-1.6E-7	2.0E-6	-1.4E-7	3.9E-6
105	9.3E-8	2.2E-6	8.6E-8	4.3E-6

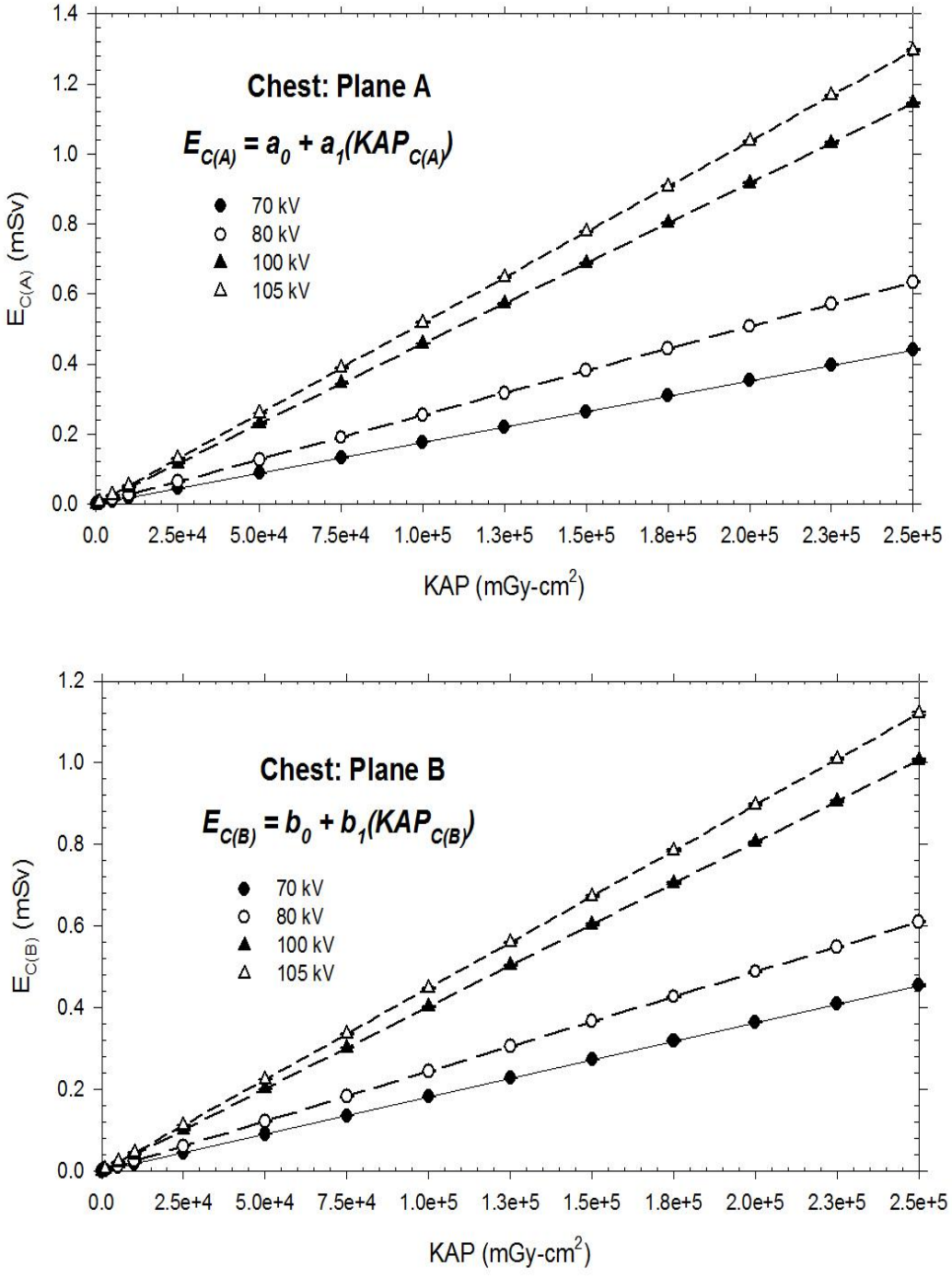

Figure 22. Effective Dose (E) in the chest region for planes A and B as a function of the incident KAP for several x-ray tube voltages.

Table 10. Figure 22 equation coefficients for planes A (AP projection) and B (lateral projection) for multiple x-ray tube voltages (kV).

X-ray Tube Voltage (kV)	Plane A		Plane B	
	a_0	a_1	b_0	b_1
70	-1.9E-7	1.8E-6	6.3E-9	1.8E-6
80	1.1E-7	2.5E-6	-1.3E-7	2.4E-6
100	1.1E-7	4.6E-6	-2.1E-8	4.0E-6
105	-8.5E-8	5.2E-6	-8.7E-8	4.5E-6

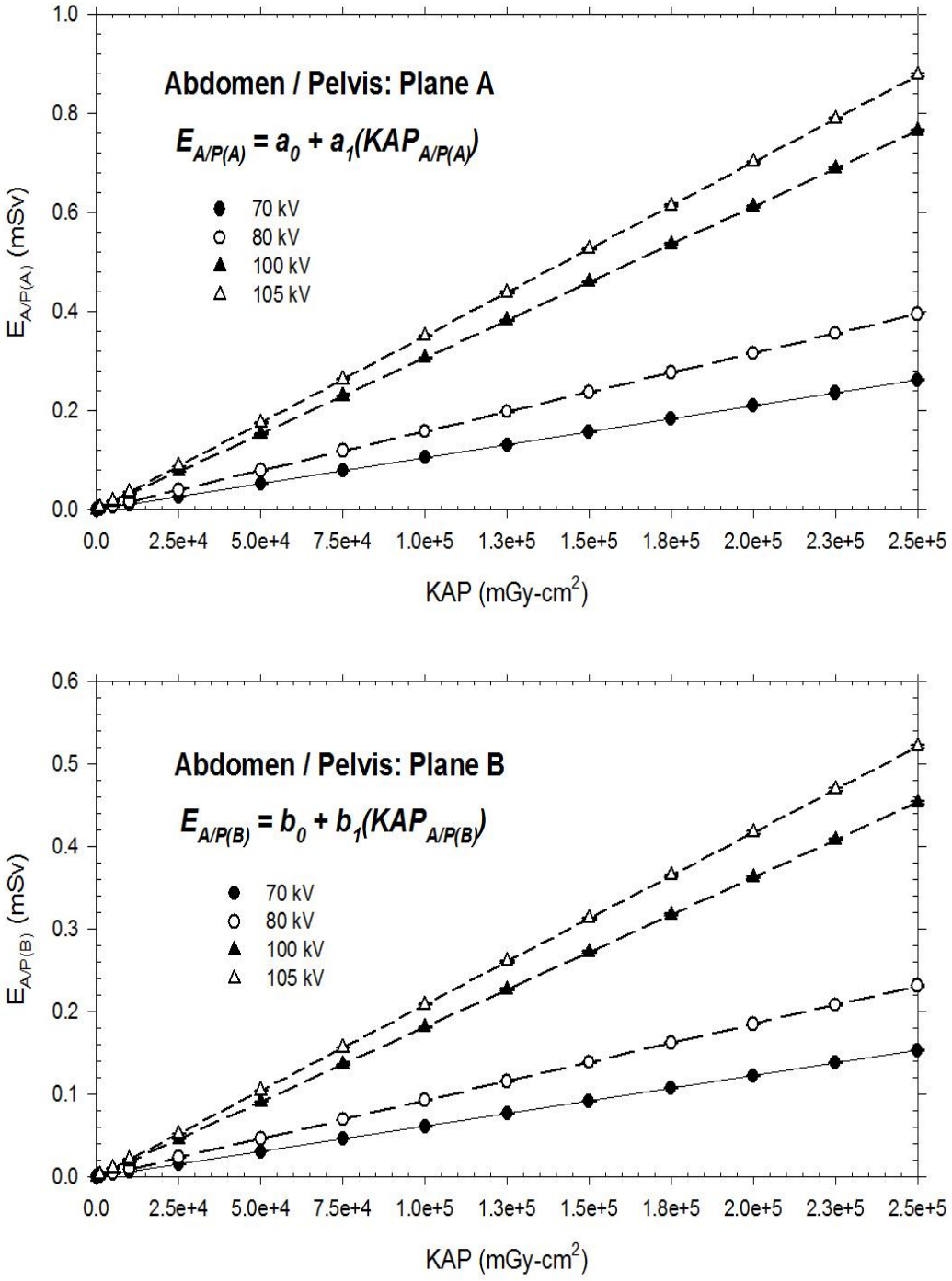

Figure 23. Effective Dose (E) in the abdomen and pelvis regions for planes A and B as a function of the incident KAP for several x-ray tube voltages.

Table 11. Figure 23 equation coefficients for planes A (AP projection) and B (lateral projection) for multiple x-ray tube voltages (kV).

X-ray Tube Voltage (kV)	Plane A		Plane B	
	a_0	a_1	b_0	b_1
70	-1.4E-7	1.0E-6	4.2E-8	6.1E-7
80	-1.1E-7	1.6E-6	9.9E-9	9.3E-7
100	1.1E-7	3.1E-6	-3.5E-8	1.8E-6
105	-7.8E-8	3.5E-6	-8.6E-8	2.1E-6

It is important to note that each plane represent a distinct projection angle and therefore has a slightly different conversion factor for Plane A versus B. The conversion factors varied by a factor of ~2 to ~4 in each plane.

Table 12 shows the minimal change in E/KAP conversion factors in the variable projection angles used in the head region during DSA imaging for Plane A.

Table 12. E/KAP (mSv/mGy·cm^2) relative to the PA for the full range of projection angles in Plane A as a function of x-ray tube voltage (kV).

	X-ray Tube Voltage (kV)			
Projection Angle	70	80	100	105
PA	1	1	1	1
10˚	1	1	1	1
20˚	1	1	1	1
30˚	1	1	1	1
40˚	1	1	1	1

Table 13 shows the same data for Plane B indicating no distinct changes in the conversion factor with only a 30 degree projection angle change.

Table 13. E/KAP (mSv/mGy·cm^2) relative to the lateral for the full range of projection angles in Plane B as a function of x-ray tube voltage (kV).

Projection Angle	X-ray Tube Voltage (kV)			
	70	80	100	105
RAO (30˚)	1	1	1	1
RAO (15˚)	1	1	1	1
Lateral	1	1	1	1
RPO (-15˚)	1	1	1	1
RPO (-30˚)	1	1	1	1

Plane B angles in the positive direction represent the II moving 15 to 30 degrees in the direction of the patient's anterior oblique. Alternatively the negative angles represent 15 to 30 degree movement towards the patient's posterior oblique angles.

To determine the thyroid organ dose the location at which the thyroid begins receiving any significant dose from scatter radiation was determined. Figure 24 illustrates the change in thyroid absorbed dose as the x-ray beam area is extended from the chest to the top of the patient's head in variable increments. The patient long axis z runs from the patient's pelvis (z = 0) to the top of the head (z = 94) and is used to describe the location of the x-ray beam and organs in the phantom. The mid-thyroid is located at z ~ 72 where the dose to the thyroid is 0.5 (50%) of the total dose. The dose to the thyroid is insignificant below z = 69 which is located in the upper chest region above the level of the female breasts.

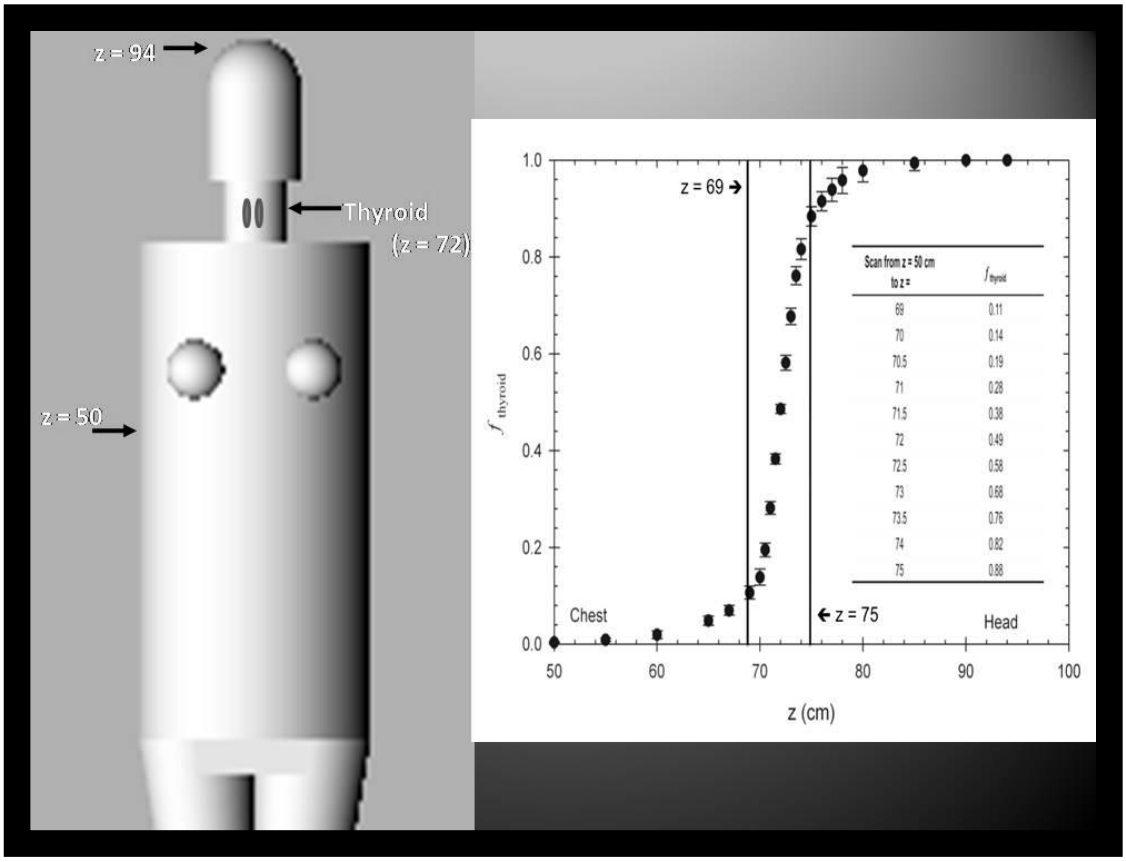

Figure 24. The fractional thyroid dose ($f_{thyroid}$) as a function of the patient long axis z (cm) showing the location of thyroid at z = 72.

Figures 25 – 27 illustrate how the thyroid organ dose (D_T) changes as a function of the KAP for several x-ray tube voltages. A least squares fit linear regression was performed for each data set and the resulting equation is also displayed. Tables 14-16 list the coefficients for each equation shown directly following the figure its shown in.

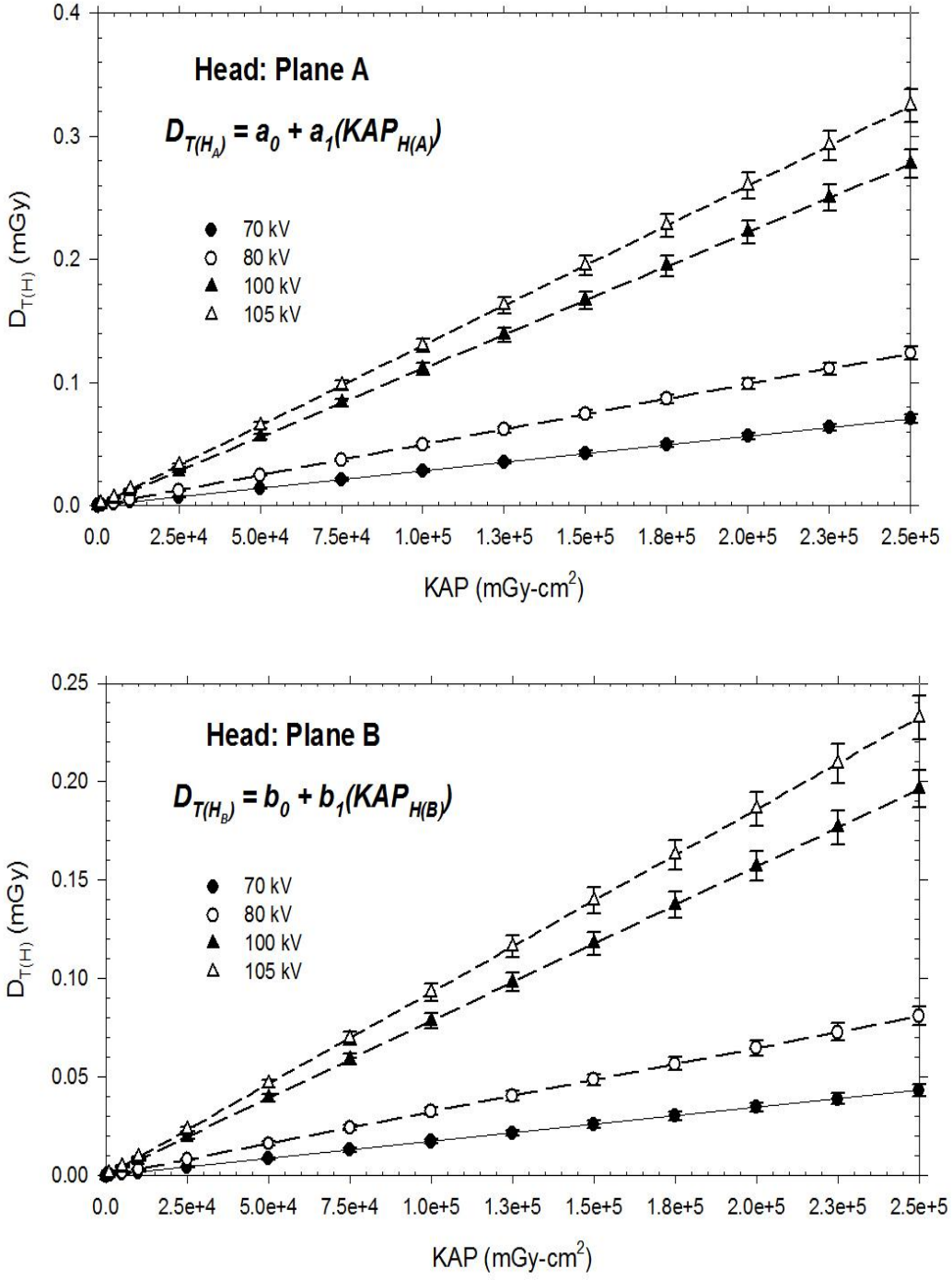

Figure 25. Thyroid Dose (D_T) in the head region for planes A and B as a function of the incident KAP for several x-ray tube voltages.

Table 14. Figure 25 equation coefficients for planes A (AP projection) and B (lateral projection) for multiple x-ray tube voltages (kV).

X-ray Tube Voltage (kV)	Plane A		Plane B	
	a_0	a_1	b_0	b_1
70	-4.1E-8	2.8E-7	9.0E-8	1.7E-7
80	-1.1E-7	4.9E-7	1.8E-8	3.2E-7
100	-9.1E-8	1.1E-6	-1.8E-7	7.8E-7
105	8.3E-8	1.3E-6	2.0E-8	9.3E-7

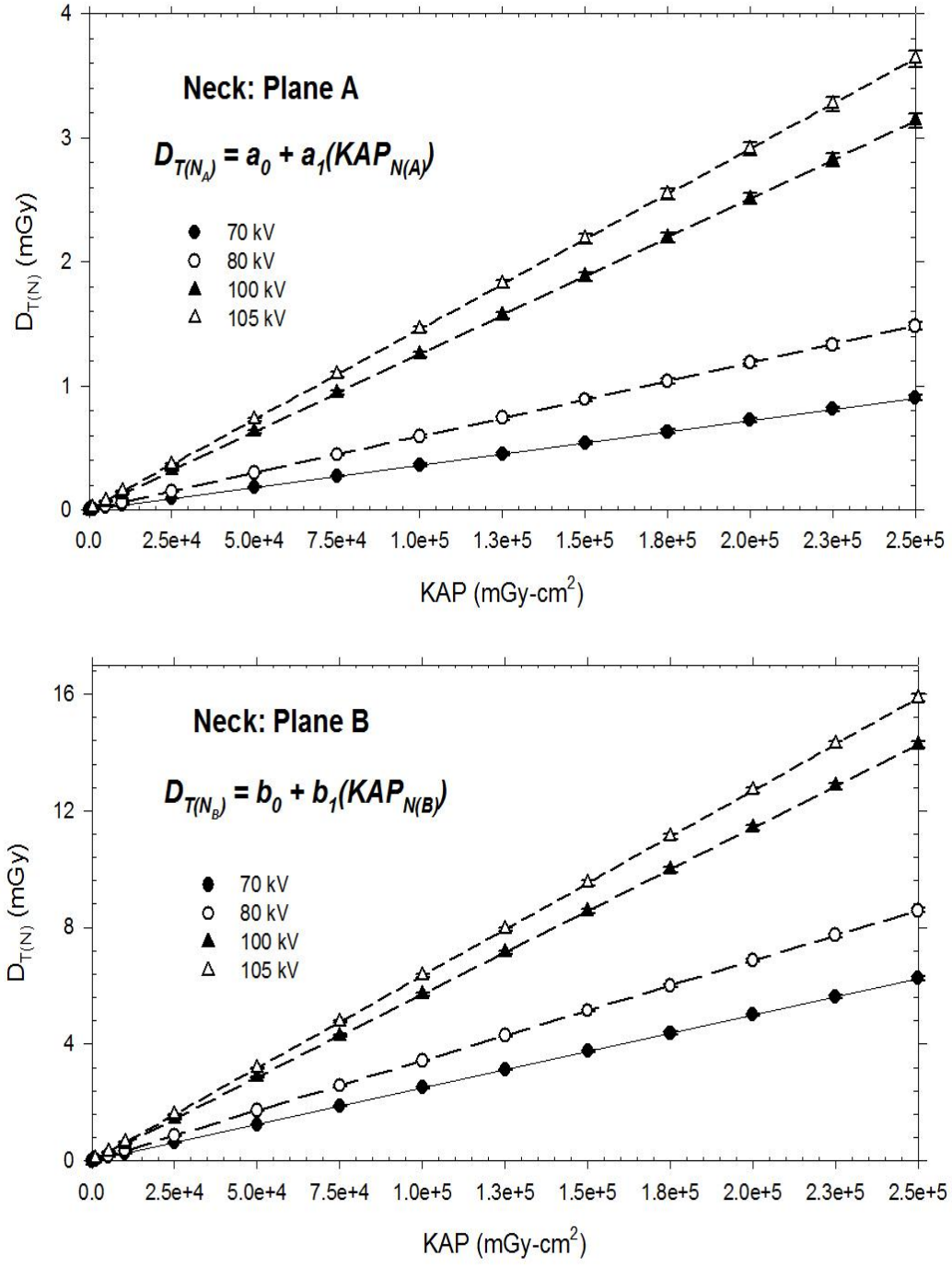

Figure 26. Thyroid Dose (D_T) in the neck region for planes A and B as a function of the incident KAP for several x-ray tube voltages.

Table 15. Figure 26 equation coefficients for planes A (AP projection) and B (lateral projection) for multiple x-ray tube voltages (kV).

X-ray Tube Voltage (kV)	Plane A		Plane B	
	a_0	a_1	b_0	b_1
70	7.1E-5	3.6E-6	3.4E-8	2.5E-5
80	-1.0E-7	5.9E-6	5.5E-8	3.4E-5
100	3.8E-8	1.3E-5	4.2E-8	5.7E-5
105	1.8E-7	1.5E-5	5.6E-8	6.3E-5

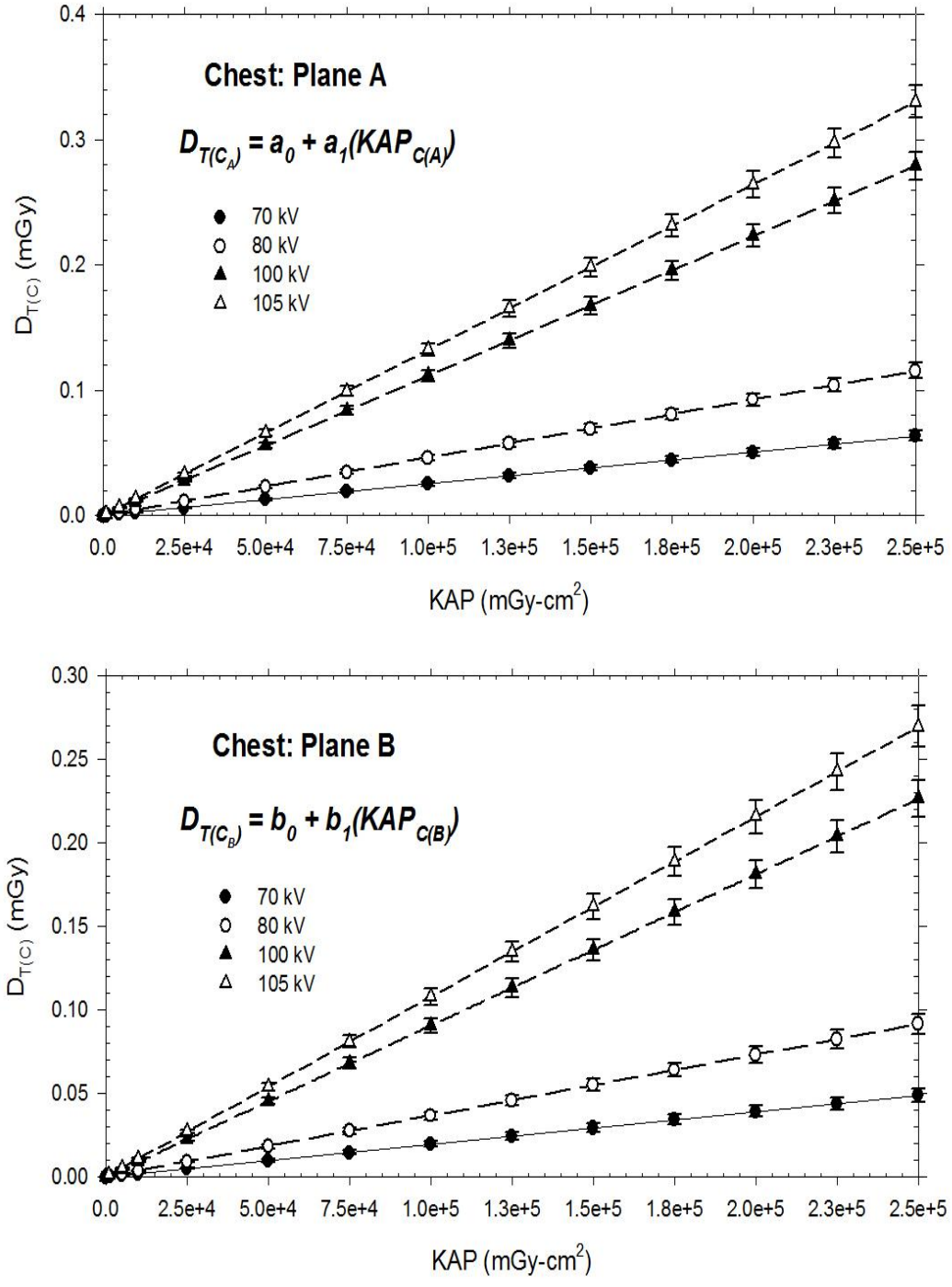

Figure 27. Thyroid Dose (D_T) in the chest region for planes A and B as a function of the incident KAP for several x-ray tube voltages.

Table 16. Figure 27 equation coefficients for planes A (AP projection) and B (lateral projection) for multiple x-ray tube voltages (kV).

X-ray Tube Voltage (kV)	Plane A		Plane B	
	a_0	a_1	b_0	b_1
70	-1.2E-7	2.5E-7	4.4E-8	2.0E-7
80	-1.5E-7	4.6E-7	7.3E-8	3.7E-7
100	2.6E-8	1.1E-6	1.7E-7	9.1E-17
105	-7.0E-8	1.3E-6	3.1E-8	1.1E-6

The thyroid dose by variable projection angle yielded the same results as the effective dose conversion factors. Tables 18 and 19 show the data for the variable angles in planes A and B for the thyroid dose conversion factors were consistent across all angles in both planes with only one exception.

Table 17. D_T/KAP (mGy/mGy·cm^2) relative to the PA for the full range of projection angles in Plane A as a function of x-ray tube voltage.

	X-ray Tube Voltage (kV)			
Projection Angle	70	80	100	105
PA	-	1	1	1
10˚	-	1	1	1
20˚	-	1	1	1
30˚	-	1	1	2
40˚	-	1	1	2

Table 18. D_T/KAP (mGy/mGy·cm^2) relative to the lateral for the full range of projection angles in Plane B as a function of x-ray tube voltage.

Projection Angle	X-ray Tube Voltage (kV)			
	70	80	100	105
RAO (30˚)	-	-	1	1
RAO (15˚)	-	-	1	1
Lateral	-	-	1	1
RPO (-15˚)	-	-	1	1
RPO (-30˚)	-	-	1	1

4.3. Stochastic Risk Conversion

Figure 19 shows the stochastic thyroid risk according to the BEIR VII data for both males and females of various ages. The data is plotted on a semi-logarithmic scale for the incidence of thyroid cancer per 100,000 cases with an absorbed organ dose of 100 mGy. A least squares fit is applied to each gender to establish a risk by age. Females exhibit an average risk ~5 times greater than their male counterparts. The risk of thyroid cancer incidence varies significantly with age by a factor of ~115 for males and ~634 for females when comparing a newborn to an 80 year old adult. Equations for quantitatively determining the risk based on patient age (years) and gender are also provided.

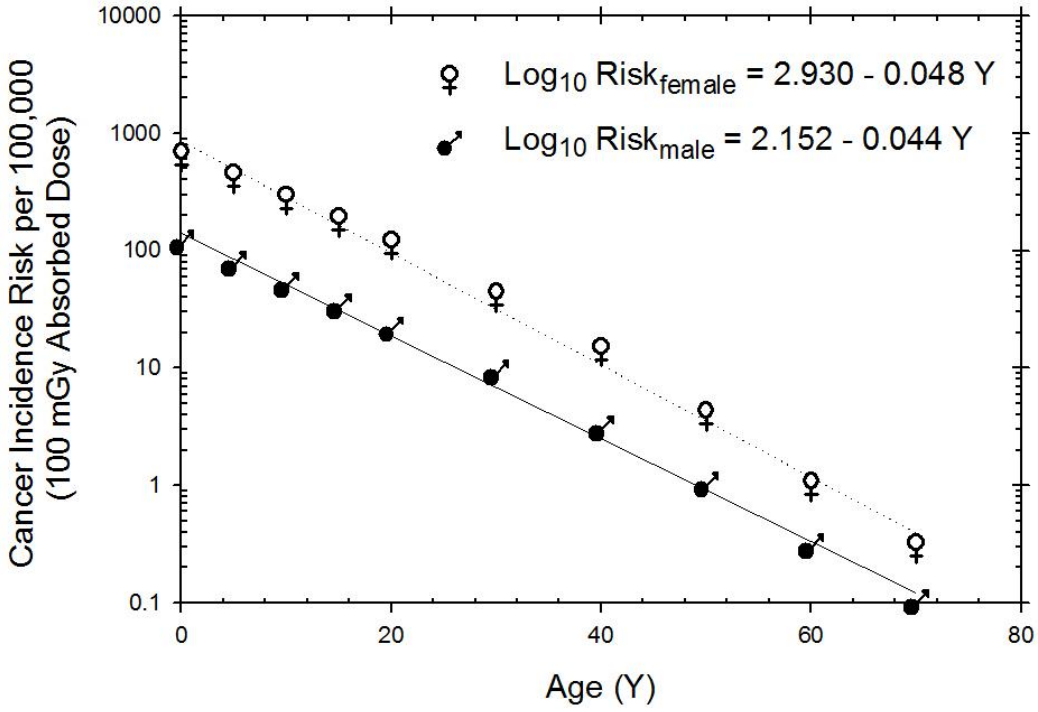

Figure 28. The Thyroid Cancer incidence risk per 100,000 cases for an absorbed dose of 100 mGy to the organ by age (years) from a newborn to geriatric adult for both males and females on a semi-logarithmic scale with a least squares fit for each sex.

5. DISCUSSION

5.1. Radiation Beam Geometry

The input parameters used to create the general dose conversion factors were taken from the radiation beam geometry established by the February cohorts studied. The dose conversion factors are more precisely simulated using the practical data obtained such as x-ray tube voltage, SID values (ie. 124 cm for Plane A and 117.5 cm for plane B), image width/height, and projection angle. The x-ray tube voltage stayed relatively consistent between the various procedures. However the voltages used in the AVM cases in plane B were more often greater than the voltages used in that plane for the other therapeutic and diagnostic procedures.

Although the image projection angles for each plane fluctuated by 40 degrees in Plane A and 30 degrees in Plane B the majority of the angles used were centered along the patient's central axis. The dose conversion factors were relatively unaffected by the change in projection angles due to the area of interest (the head) being a symmetric structure with fewer vital organs affecting the conversion factors than would be the case in an area of interest in the chest, abdomen and pelvis regions. Since the fluoroscopy imaging through the trunk region was limited to catheter placement and guidance through larger arteries and veins multiple angles in each plane would be unnecessary. Therefore, the AP and lateral angle for each plane was used to create these conversion factors.

The total fluoroscopy KAP in each body region will be important in determining an accurate effective dose, and thyroid organ dose as the imaging region approaches the neck. Other researchers have suggested

conversion factors to account for patient weight as well, since the phantom used in the simulations is a standard size and many patients are either smaller or larger which will subsequently affect the calculated dose. However due to the limited imaging in the body region and the majority of the imaging in the head region reasonable correction factors would be challenging to assume for effective dose in the patient's head and neck regions and most likely un-necessary for the limited imaging in the body.

5.2. Effective and Organ Dose Conversion

The effective dose (E) in mSv can be calculated as a function of the total KAP for each plane using the E/KAP conversion factors shown in Figures 20 - 23. Using KAP as an indicator has been shown in several studies to be accurate for effective dose and organ dose, but not for skin doses.[44,45] The access points for the catheter and guide wire insertions are typically located in the patient's groin area (femoral vein). Some of the attributable dose will also come from the fluoroscopy performed in the chest, abdomen, and pelvis, therefore, it is important to take the KAP incident on the patient in these regions into account when calculating the effective dose. The conversion factors will be greater in the trunk region of the body due to the larger number of radiation sensitive organs that will be exposed in the beam for plane A. Since plane B is located laterally instead of posterior to the patient, the chest and neck area will have the greatest conversion factors.

The total KAP by plane and for each imaging area should be accounted for to accurately estimate the effective dose. The procedures increase in complexity as the wires are navigated towards the head, so it is likely that the imaging will be greater in the chest than in the lower trunk regions (ie. abdomen and pelvis). In planes A and B the conversion factors

for the abdomen and pelvis could be assumed to be constant with the chest due to the limited imaging in that region. Also the neck conversion factors could be used for imaging in the head and neck region, since the thyroid is the main tissue driving the effective dose in that region and it will receive some dose from imaging in the head region due to scatter radiation. These simplifications would allow the user to split the total KAP into one dose for the trunk and one dose for the head/neck. The most accurate doses will be achieved by accounting for the KAP at each region and at each x-ray tube voltage, so this simplification would obviously introduce some uncertainty into the calculation, but it would also most likely overestimate the effective dose. This also makes E easier and more efficient for Interventionalists to calculate post procedure.

The thyroid dose can be calculated using the D_T/KAP conversion factors from Figures 25 - 27 if the total KAP for head, neck and chest regions are known for planes A and B. A small percentage of the procedure will be focused in the chest, abdomen, and pelvis for the catheter insertion and guidance. However, the DSA imaging will be almost exclusively focused in the head and neck regions. Since the dose to the thyroid will vary depending on the imaging region (as shown in Figure 24) the KAP accumulated in the abdominal and pelvic regions will account for less than 1% of the thyroid organ dose, therefore, the KAP from this area can be neglected in the calculations.

The entrance and exit location of the x-ray beam will vary depending on the angle used during each imaging run. Tables 12 and 13 show the relative D_T/KAP conversion factors for the variety of angles the x-ray tube assembly is capable of in each plane. In plane A the x-ray tube is in the posterior position with the II located anterior to the patient. This plane can

rotate up to 40˚, hence, the x-ray beam entrance will always be from the posterior, so the conversion factor was normalized to the posteroanterior (PA) projection. At 105 kV if the assembly is rotated 30˚ to 40˚ then the conversion factor will be a factor of 2 greater than in the PA. According to Figure 19, less than 7% of the total imaging runs, regardless of x-ray tube voltage, were conducted at those angles. In plane B table 18 shows no appreciable difference in the conversion factor by projection angle, so the conversion factors from Figures 25 - 27 can be used for all angles.

Appendix D shows some example effective doses and thyroid organ doses using the DSA and fluoroscopy data collected in Table 6. For these calculations it was assumed that all the fluoroscopy KAP was concentrated in the patient's trunk region and the DSA KAP was in the head and neck region. The effective dose simplifications described earlier were also used. An x-ray tube voltage of 105 kV in plane A and 70 kV in plane B were also assumed using the data from Figure 13. The average effective dose using this method was 0.5 ± 0.7 mSv and the average thyroid dose was 2.2 ± 2.3 mGy. This effective dose for one procedure alone is roughly half the annual limit (1.0 mSv) for a member of the public.[46] Effective doses in the literature for head and neck angiography have been reported between 0.8 – 19.6 mSv, but these doses vary greatly depending on the skill of the operator and the dose reduction methods used as well as the complexity of the procedure.[47] Also using the theory that the Interventionalist's eye dose can be calculated as 75% of the patient's thyroid dose yields a dose of ~1.7 mGy to the Interventionalists eyes.[39] The doses estimated in Appendix D are taken from 14 treatment and 16 diagnostic procedures with an average fluoroscopy time of 49 minutes. Interestingly the majority of these cases were performed by the same Interventionalist. The lower doses could be indicative of good radiation reduction techniques used in the procedures, or

simply shorter less complex procedures in this particular group. Tracking this data over a greater length of time would allow the institution to determine the cause of these low doses and to identify any particular practices or individuals that may need radiation reduction method improvements.

5.3. Stochastic Risk Conversion

Appendix D illustrates the potential thyroid cancer risk per 100,000 cases for both males and females ranging in age from 25 to 65 years old for the data gathered in Table 6. There would be little disagreement about the stochastic effects of ionizing radiation at thyroid doses of several Gray (Gy), however, as the thyroid dose is progressively reduced, the empirical evidence of thyroid cancer risk gradually diminishes. As the empirical data diminishes, controversies regarding radiation risks generally increase.[48-50] BEIR VII explicitly provides risk estimates for thyroid organ doses of 100 mGy to alert users that any extrapolation of thyroid risks to lower levels would be associated with large uncertainties. The quantitative thyroid risk estimates obtained using the approach proposed in this paper are reflective of the best available understanding of radiation carcinogenesis, as reflected by recent reports released by BEIR, ICRP and UNSCEAR.[30, 51-52]

6. CONCLUSION

Doses in INR can be reduced by adhering to good radiation safety practices. When the operating staff is appropriately trained and informed of the potential dose saving not only for the patient but also to the operators then the potential stochastic and non-stochastic risks can be reduced as well. Dose reduction methods such as last image hold, and pulsed fluoroscopy acquisition, which acquires slightly less than real time imaging

(< 30 frames per second) along with the understanding that DSA acquisitions generally translate into higher doses to the patient than fluoroscopy acquisitions will aid operators in reducing doses. Institutions trying to ensure patient safety in INR will need to have a method to quantify the doses imparted to the patients during these procedures so that standards within the institution can be set, and also so areas of improvement can be identified.

INR procedures have the potential for high radiation doses to patients (0.8 – 19.6 mSv).[47] Without adequate dose estimation patients may receive greater doses than are actually needed. Patients undergoing multiple INR procedures are especially at risk for increasing stochastic risks as radiation effects are compounded over time. If patients are not monitored then it becomes increasingly challenging for the patient and physician to access the potential risk to benefit a particular procedure will provide. Providing a quick and simple radiation dose estimation tool for Interventionalists will aide in their compliance with ALARA standards and institutions to remain compliant with the Joint Commission standards of cumulative doses lower than 15 Gy to any one particular area. This tool will assist them in providing safer INR procedures for their patient's by reducing non-stochastic and stochastic risks. Thereby maximizing the benefits of the procedure and minimizing the radiation dose risk.

Bibliography

1. Radiology Info: The Radiology Information Resource for Patients. *Glossary of Terms*. Chicago: Radiological Society of North America, Inc. ; 2010
2. Rosch J, Keller FS, Kaufman JA. The birth, early years, and future of interventional radiology. *J Vasc Interv Radiol* 2003;14:841-853
3. SIR. The History of Interventional Radiology. *Interventional Radiologists are Minimally Invasive Specialists*. Fairfax: Society of Interventional Radiology; 2010
4. SIR. In: Radiology SoI, ed. Fairfax: Society of Interventional Radiology; 2010
5. Faulkner K. Radiation protection in interventional radiology. *Br J Radiol* 1997;70:325-326
6. Practice Guidelines for Interventional Clinical Practice. American College of Radiology; 2009:1-9
7. National Council on Radiation Protection and Measurements., Scientific Committee 6-2 on Radiation Exposure of the U.S. Population. *Ionizing radiation exposure of the population of the United States : recommendations of the National Council on Radiation Protection and Measurements*. Bethesda, Md.: NCRP; 2009
8. SNIS. In: SNIS, ed. Fairfax: Society of Neurointerventional Surgery; 2008:website
9. Harrigan MR. *Handbook of cerebrovascular disease and neurointerventional technique*. New York: Springer; 2008
10. Willinsky RA, Taylor SM, TerBrugge K, et al. Neurologic complications of cerebral angiography: prospective analysis of 2,899 procedures and review of the literature. *Radiology* 2003;227:522-528
11. Endarterectomy for asymptomatic carotid artery stenosis. Executive Committee for the Asymptomatic Carotid Atherosclerosis Study. *JAMA* 1995;273:1421-1428
12. Bhatt DL. *Guide to peripheral and cerebrovascular intervention*. London: Remedica Publishing; 2004
13. Lyden PD. *Thrombolytic therapy for stroke*. Totowa, N.J.: Humana Press; 2001
14. Marotta TR, Gunnarsson T, Penn I, et al. A novel endovascular clip system for the treatment of intracranial aneurysms: technology, concept, and initial experimental results. Laboratory investigation. *J Neurosurg* 2008;108:1230-1240
15. Stieg PE, Batjer HH, Samson DS. *Intracranial Arteriovenous Malformations*. Richmond: Informa Healthcare 2007

16. Abrams HL, Baum S, Pentecost MJ. *Abrams' angiography : interventional radiology*. Philadelphia, Pa. ; London: Lippincott Williams & Wilkins; 2006
17. Massoud TF, Hademenos GJ. Transvenous retrograde nidus sclerotherapy under controlled hypotension (TRENSH): a newly proposed treatment for brain arteriovenous malformations--concepts and rationale. *Neurosurgery* 1999;45:351-363; discussion 363-355
18. Heuser RR, Henry MMD. *Textbook of peripheral vascular interventions*. London: Informa Healthcare; 2008
19. Greenberg MSMD. *Handbook of neurosurgery*. Lakeland, FL: Greenberg Graphics ; New York : Thieme Medical Publishers; 2006
20. Hurst RW, Rosenwasser RH. *Interventional neuroradiology*. New York: Informa Healthcare; 2008
21. Solutions SAM. Axiom Artis FA/BA Operating Manual. Germany; 2003
22. Huda W. *Review of radiologic physics*. Baltimore, MD: Lippincott Williams & Wilkins; 2010
23. Curry TS, Dowdey JE, Murry RC, et al. *Christensen's physics of diagnostic radiology*. Philadelphia: Lea & Febiger; 1990
24. Jacobson B, Murray A. Medical Devices Slides: Use and Safety. Elsevier; 2006
25. Miller DL, Balter S, Wagner LK, et al. Quality improvement guidelines for recording patient radiation dose in the medical record. *J Vasc Interv Radiol* 2009;20:S200-207
26. Stecker MS, Balter S, Towbin RB, et al. Guidelines for patient radiation dose management. *J Vasc Interv Radiol* 2009;20:S263-273
27. Huda W. Medical Radiation Dosimetry. *RSNA Categorical Course in Diagnostic Radiology Physics: From Invisible to Visible- The Science and Practice of X-ray Imaging and Radiation Dose Optimization*; 2006:29-39
28. Balter S. Methods for measuring fluoroscopic skin dose. *Pediatr Radiol* 2006;36 Suppl 2:136-140
29. Beutel J. *Handbook of medical imaging*. Bellingham, Wash.: SPIE Press; 2000
30. The 2007 Recommendations of the International Commission on Radiological Protection. ICRP publication 103. *Ann ICRP* 2007;37:1-332
31. Hall EJ, Giaccia AJ. *Radiobiology for the radiologist*. Philadelphia: Lippincott Williams & Wilkins; 2006
32. Administration FaD. Public Health Advisory: avoidance of a seriousx-ray-induced skin injuries to patients during fluoroscopically-guided procedures. Rockville, MD: Center for Devices and Radiological Health; 1994
33. 10CFR20.1201: Occupational Dose Limits for Adults. In: Commission NR, ed.

34. Siiskonen T, Tapiovaara M, Kosunen A, et al. Occupational radiation doses in interventional radiology: simulations. *Radiat Prot Dosimetry* 2008;129:36-38
35. Radiology ACo. Practice Guideline for the Reporting and Archiving of Interventional Radiology Procedures. Revised 2009 (Res. 23). 2006
36. Miller DL, Kwon D, Bonavia GH. Reference levels for patient radiation doses in interventional radiology: proposed initial values for U.S. practice. *Radiology* 2009;253:753-764
37. Commission TJ. Sentinel Events Policies and Procedures. July 2007
38. Balter S, Hopewell JW, Miller DL, et al. Fluoroscopically guided interventional procedures: a review of radiation effects on patients' skin and hair. *Radiology* 2010;254:326-341
39. Clerinx P, Buls N, Bosmans H, et al. Double-dosimetry algorithm for workers in interventional radiology. *Radiat Prot Dosimetry* 2008;129:321-327
40. National Academy of Sciences Committee on the Biological Effects of Ionizing Radiation (BEIR) Report VII. Health Effects of Exposure to Low Levels of Ionizing Radiations: Time for Reassessment? Washington DC; 2005
41. Tapiovaara M, Lakkisto M, Servomaa A. PCXMC- A PC-based Monte Carlo program for calculating patient doses in medical x-ray examinations. Finnish Centre for Radiation and Nuclear Safety (STUK), Helsinki, 1997.
42. Cristy M. Mathematical Phantoms Representing Children of Various Ages Fore Use in Internal Dose. In: Division HaSR, ed.: ORNL; 1980
43. PCXMC Version 2.0; released 2008; STUK, Finland.
44. Yakoumakis E, Tsalafoutas IA, Nikolaou D, et al. Differences in effective dose estimation from dose-area product and entrance surface dose measurements in intravenous urography. *Br J Radiol* 2001;74:727-734
45. Bor D, Sancak T, Olgar T, et al. Comparison of effective doses obtained from dose-area product and air kerma measurements in interventional radiology. *Br J Radiol* 2004;77:315-322
46. 10CFR20.1301: Dose Limits for Individual Members of the Public.
47. Mettler FA, Jr., Huda W, Yoshizumi TT, et al. Effective doses in radiology and diagnostic nuclear medicine: a catalog. *Radiology* 2008;248:254-263
48. Evaluation of the Linear-nonthreshold dose-response model for ionizing radiation: Recommendations of the National Council on Radiation Protection and Measurement. *NCRP Report No 136*. Bethesda; 2001:287
49. Upton AC. The state of the art in the 1990's: NCRP Report No. 136 on the scientific bases for linearity in the dose-response relationship for ionizing radiation. *Health Phys* 2003;85:15-22
50. Preston RJ. The LNT model is the best we can do--today. *J Radiol Prot* 2003;23:263-268

51. Health effects of exposure to low levels of ionizing radiations: Time for reassessment? *National Academy of Sciences Committee on the Biological Effects of Ionizing Radiation (BEIR)* 2005;Report No. VII
52. UNSCEAR. UNSCEAR 2006 Report. Annex A. Epidemiological Studies of Radiation and Cancer. In: Nations U, ed. New York; 2008

APPENDIX A.

Units of radiation measurement[22]

Quantity	SI Unit	Non-SI Unit	Non-SI → SI Conversion
Exposure	C / Kg	Roentgen (R)	$1R = 2.58x10^{-4}$ C/Kg
Air KERMA	Gray (Gy)	Roentgen (R)	1R = 8.76 Gy
Absorbed Dose	Gray (Gy)	Rad (100 erg/g)	1 rad = 100 Gy
Equivalent Dose	Sievert (Sv)	Rem	1 rem = 100 Sv
KAP	$Gy\text{-}cm^2$	-	-
IRP Dose	Gray (Gy)	-	-
Effective Dose	Sievert (Sv)	Rem	1 rem = 100 Sv

APPENDIX B.

Anthropomorphic phantom used by PCXMC 2.0 based on the 1987 Cristy and Eckerman phantom.

Age	Height (cm)	Weight (kg)
Newborn	50.9	3.4
10 y	139.8	32.4
15 y	168.1	56.3
Adult	178.6	73.2

PCXMC geometries for planes A and B used in the simulations (BW is beam width, BH is beam height, and z is the patient long axis reference).

Plane A (cm)				
SID	124 max	109	94 min	
Image Width	32			
Image Height	32			
Anode Angle	12˚			
Head				
Angle	FSD	BW	BH	z
90	72.17	18.63	18.63	88
100	71.40	18.43	18.43	88
110	71.83	18.54	18.54	88
120	72.44	18.69	18.69	88
130	73.10	18.87	18.87	88
Body Regions				
Region	FSD	BW	BH	z
Neck	70.00	18.06	18.06	75
Chest	70.00	27.10	27.10	54
Abdomen/Pelvis	70.00	27.10	40.00	18

Plane B (cm)				
SID	117.5 max		102.5	87.5 min
Image Width	25			
Image Height	25			
Anode Angle	12˚			
Head				
Angle	FSD	BW	BH	z
330	73.74	15.69	15.69	89
345	74.39	15.83	15.83	89
0	74.00	15.74	15.74	89
15	74.29	15.81	15.81	89
30	73.74	15.69	15.69	89
Body Regions				
Region	FSD	BW	BH	z
Neck	79.20	16.85	16.85	75
Chest	50.00	20.43	25.00	55
Abdomen/Pelvis	50	20.43	40	18

APPENDIX C. Radiation Geometry by INR Procedure

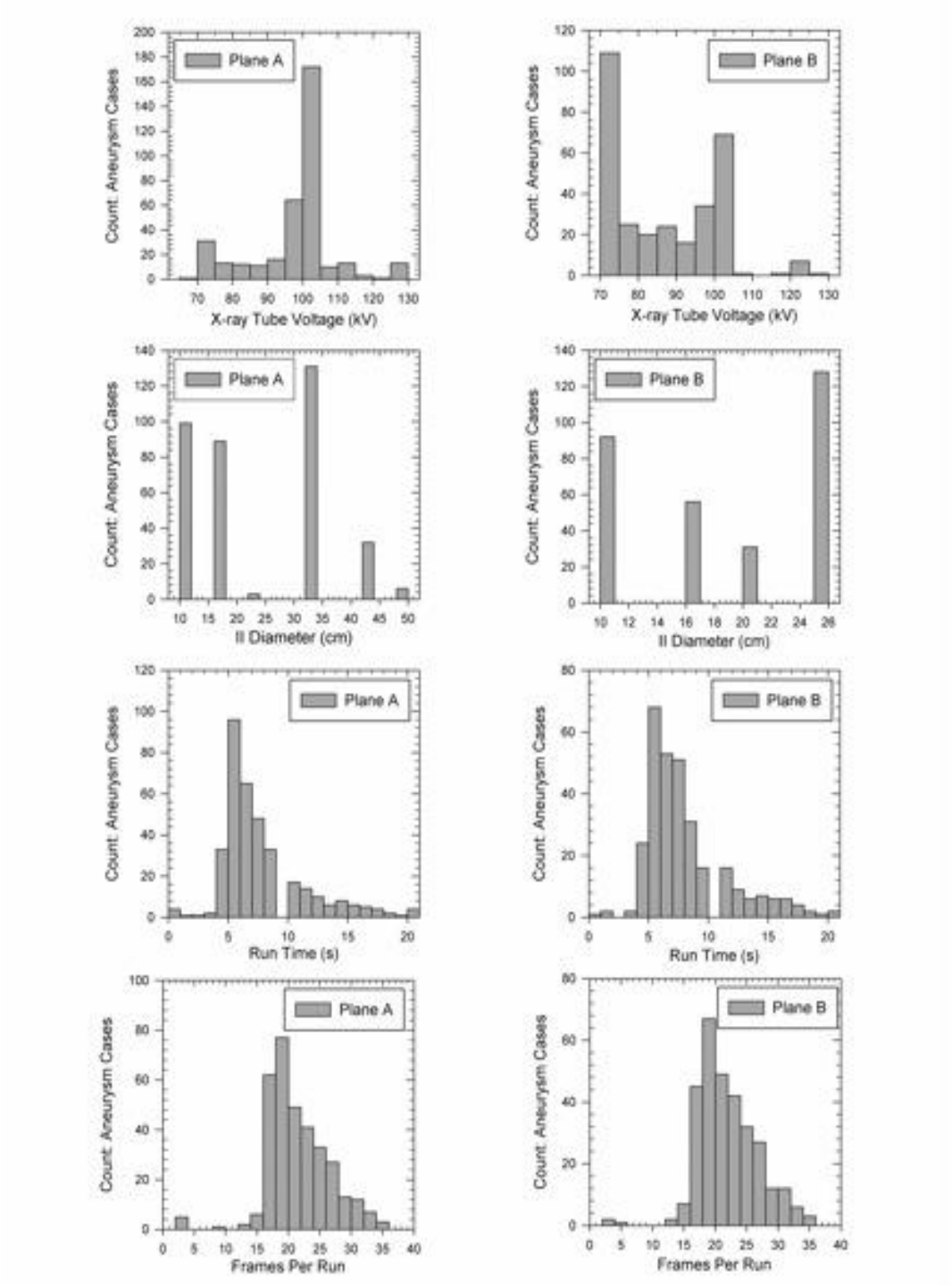

Figure 29. Radiation beam geometry for all Aneurysm cases performed in February 2010 at MUSC.

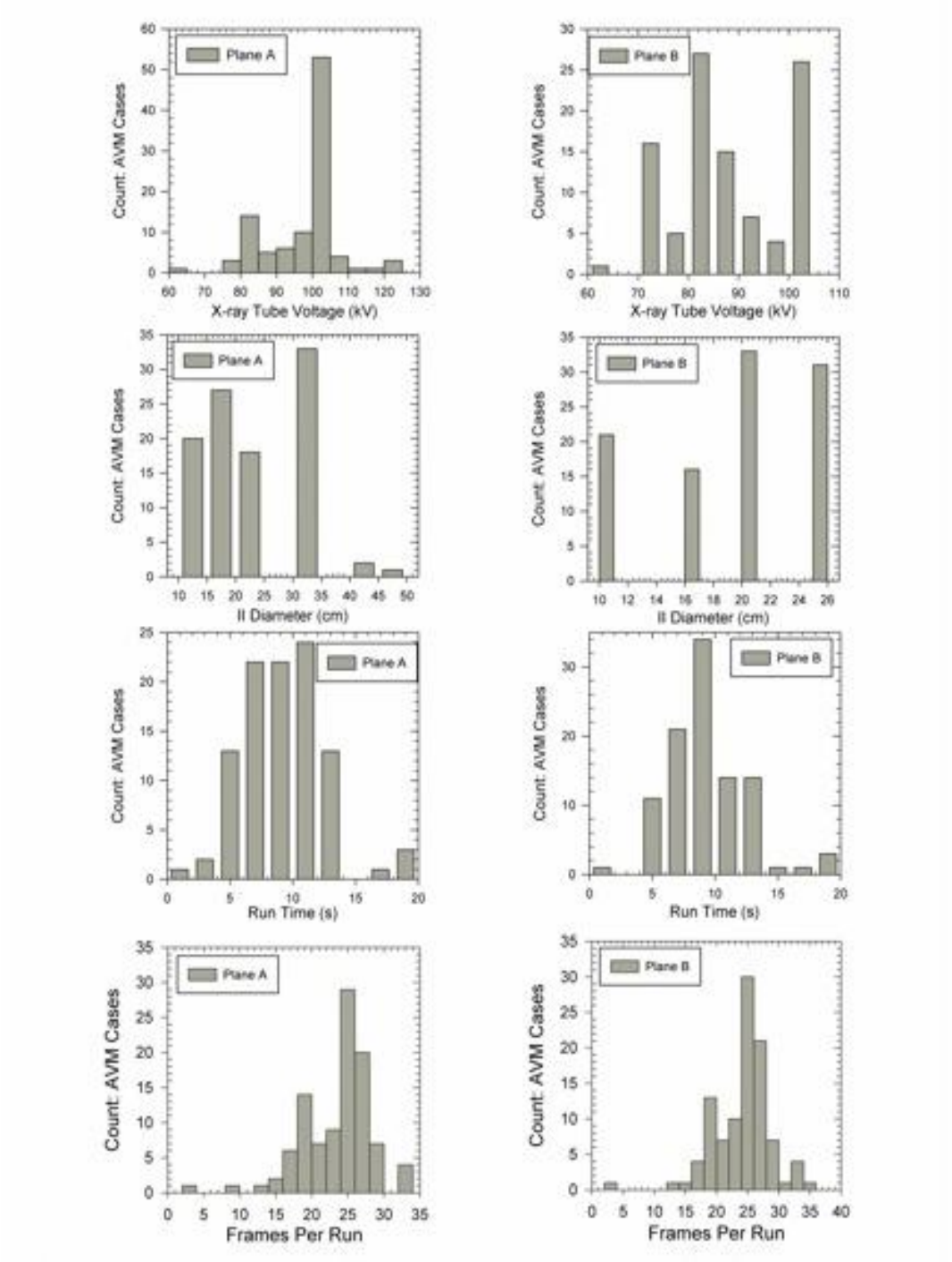

Figure 30. Radiation beam geometry for all AVM cases performed in February 2010 at MUSC.

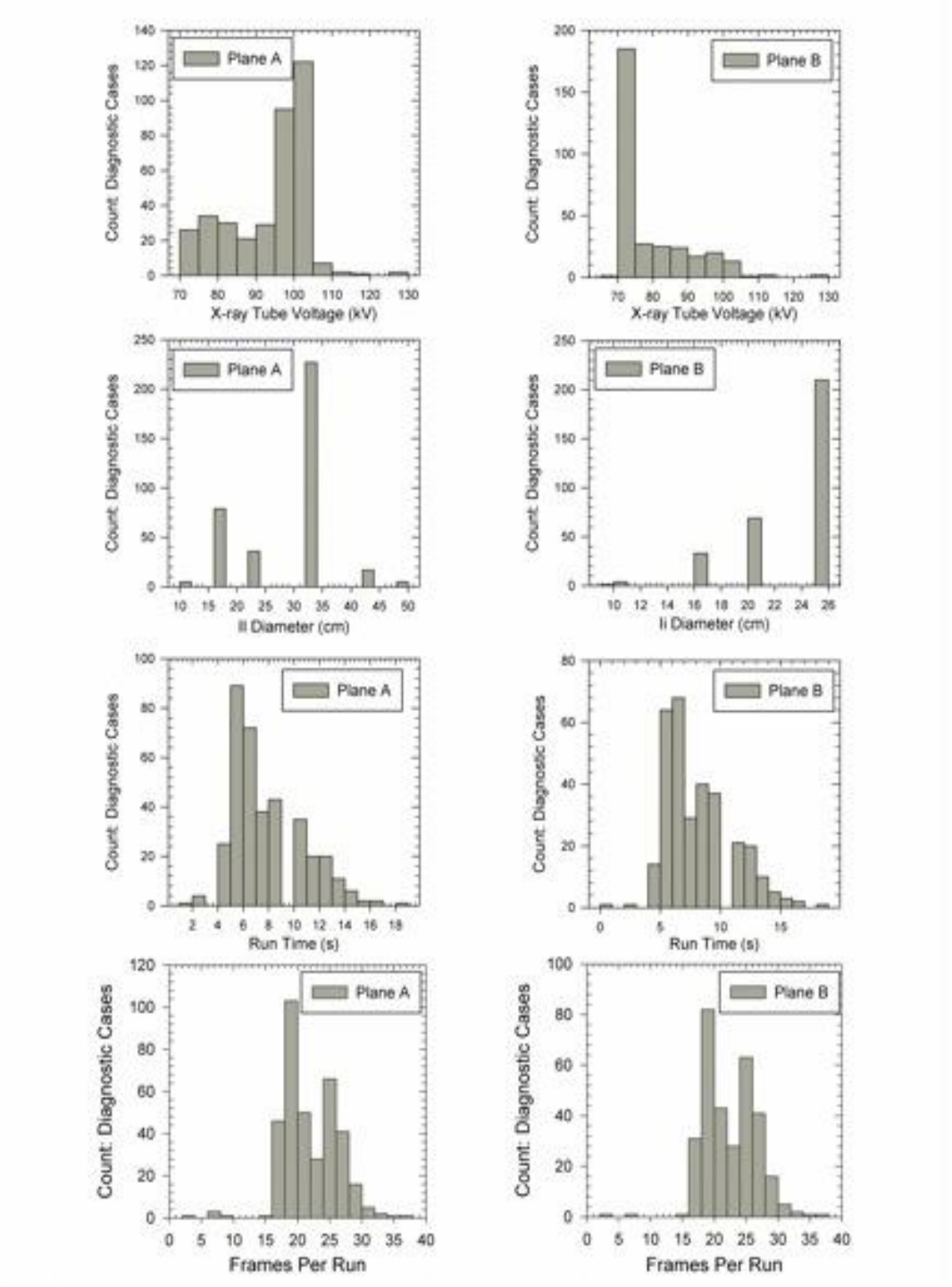

Figure 31. Radiation beam geometry for all diagnostic Angioplasty cases performed in February 2010 at MUSC.

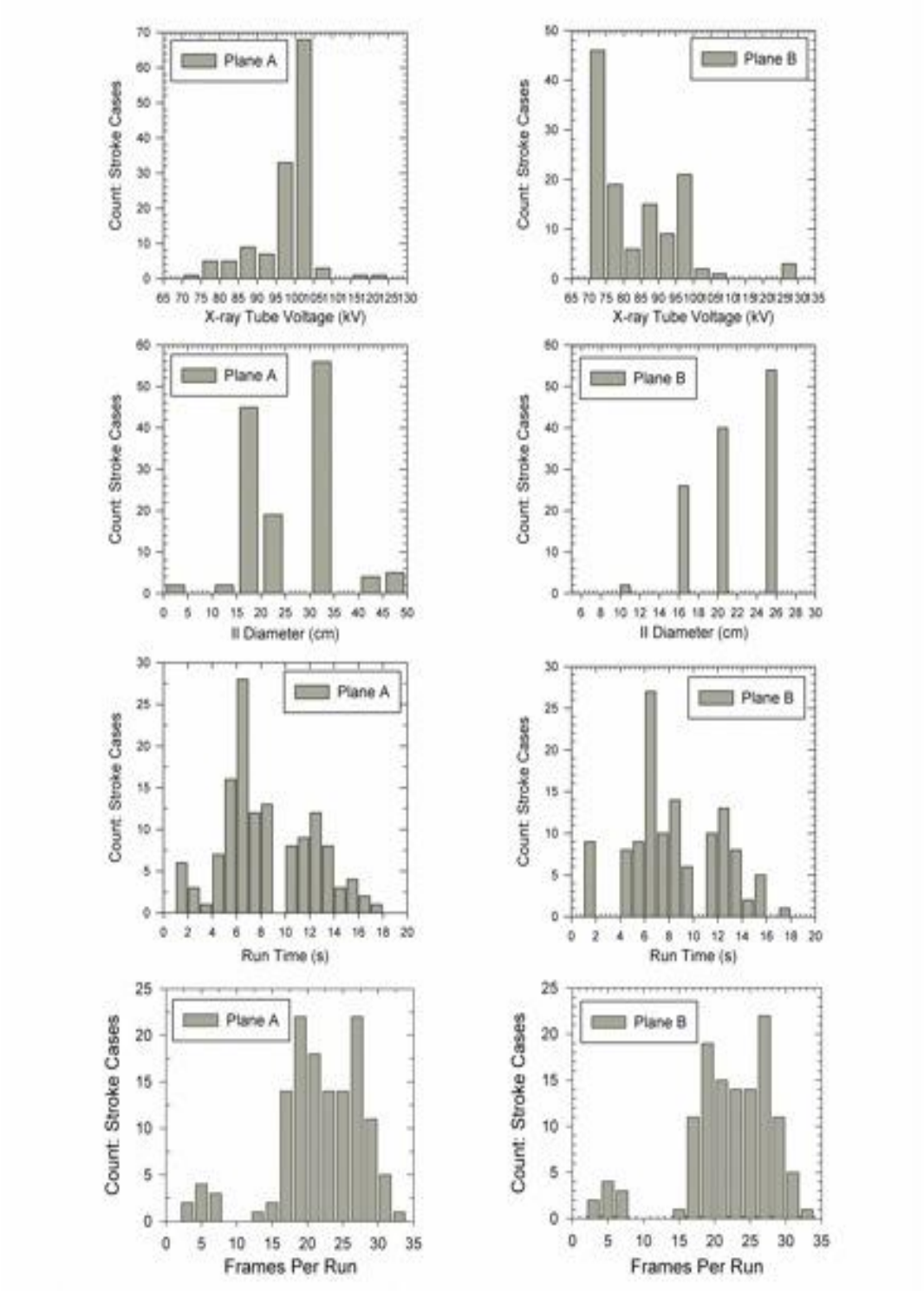

Figure 32. Radiation beam geometry for all Stroke Therapy cases performed in February 2010 at MUSC.

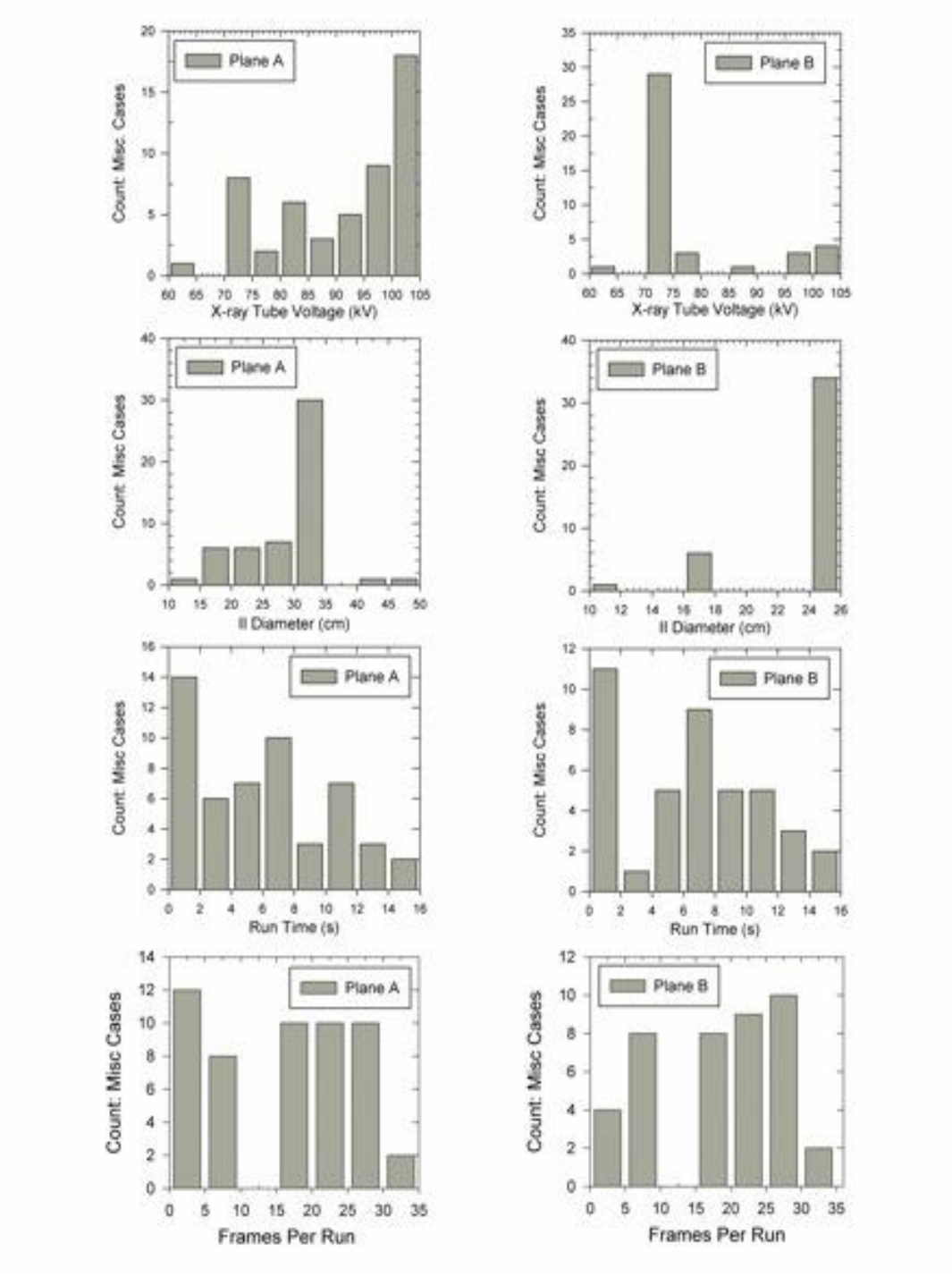

Figure 33. Radiation beam geometry for all miscellaneous cases (ie. Vasospasm, Sclerotherapy, etc.) performed in February 2010 at MUSC.

APPENDIX D. E, D_T, and R_P INR Calculations

$$E = \sum E_H + \sum E_N + \sum E_C + \sum E_{A/P}$$

	A (mSv)			B (mSv)			E
	DSA	F	Total	DSA	F	Total	(mSv)
	0.14	0.03	0.17	0.06	0.00	0.06	0.23
	0.08	0.03	0.12	0.04	0.00	0.05	0.16
	0.29	0.11	0.40	0.08	0.01	0.09	0.49
	0.30	0.41	0.71	0.19	0.05	0.24	0.95
	0.24	0.32	0.56	0.05	0.04	0.10	0.66
	0.35	0.66	1.00	0.13	0.13	0.26	1.27
	0.15	0.07	0.22	0.06	0.00	0.06	0.29
	0.18	0.28	0.46	0.07	0.03	0.10	0.57
	0.08	0.02	0.10	0.03	0.00	0.03	0.13
	0.24	0.11	0.35	0.08	0.01	0.09	0.44
	0.46	0.58	1.04	0.09	0.04	0.13	1.17
	0.18	0.07	0.24	0.06	0.00	0.07	0.31
	0.17	0.11	0.28	0.07	0.01	0.08	0.36
	0.26	0.34	0.60	0.07	0.05	0.12	0.72
	0.14	0.29	0.43	0.05	0.00	0.05	0.48
	0.10	0.04	0.13	0.03	0.00	0.04	0.17
	0.16	1.09	1.25	0.07	0.17	0.24	1.49
	0.06	0.04	0.10	0.02	0.00	0.03	0.12
	0.24	0.69	0.93	0.08	0.00	0.08	1.01
	0.17	0.11	0.27	0.06	0.01	0.06	0.34
	0.20	0.11	0.31	0.09	0.01	0.10	0.41
	0.04	0.01	0.05	0.01	0.00	0.01	0.06
	0.15	0.10	0.25	0.07	0.00	0.07	0.32
	0.06	0.05	0.11	0.01	0.00	0.02	0.12
	0.07	0.09	0.16	0.03	0.00	0.03	0.19
	0.15	0.15	0.30	0.04	0.02	0.06	0.37
	0.29	0.19	0.48	0.08	0.01	0.09	0.57
	0.15	0.21	0.37	0.05	0.01	0.06	0.43
	0.14	0.23	0.37	0.04	0.02	0.06	0.44
	0.21	0.24	0.45	0.07	0.02	0.08	0.54
Average	0.18	0.23	0.41	0.06	0.02	0.09	0.49
(± 2σ)	(0.19)	(0.49)	(0.61)	(0.07)	(0.08)	(0.12)	(0.72)

E (mSv): Patient effective doses calculated for DSA and Fluoroscopy (F) runs as a function of the plane. The total E for both planes and all runs are also shown.

$$D_T = \sum D_{T(H)} + \sum D_{T(N)} + \sum D_{T(C)}$$

A (mGy)			B (mGy)			D_T
DSA	F	Total	DSA	F	Total	(mGy)
0.96	0.01	0.96	0.91	0.00	0.91	1.87
0.56	0.01	0.56	0.65	0.00	0.65	1.21
2.01	0.03	2.04	1.12	0.00	1.12	3.16
2.06	0.10	2.17	2.80	0.01	2.80	4.97
1.64	0.08	1.72	0.81	0.00	0.81	2.54
2.37	0.16	2.54	1.94	0.01	1.95	4.49
1.03	0.02	1.05	0.90	0.00	0.90	1.95
1.23	0.07	1.30	1.10	0.00	1.10	2.40
0.53	0.01	0.54	0.45	0.00	0.45	0.99
1.62	0.03	1.65	1.14	0.00	1.14	2.79
3.11	0.14	3.26	1.30	0.00	1.30	4.56
1.20	0.02	1.22	0.91	0.00	0.91	2.13
1.19	0.03	1.22	0.99	0.00	0.99	2.21
1.78	0.08	1.86	0.99	0.01	1.00	2.86
0.95	0.07	1.02	0.70	0.00	0.70	1.72
0.67	0.01	0.68	0.49	0.00	0.50	1.17
1.11	0.27	1.38	1.04	0.02	1.06	2.44
0.41	0.01	0.42	0.37	0.00	0.37	0.78
1.64	0.17	1.81	1.14	0.00	1.14	2.94
1.13	0.03	1.16	0.86	0.00	0.86	2.02
1.34	0.03	1.37	1.35	0.00	1.35	2.72
0.24	0.00	0.24	0.10	0.00	0.10	0.35
1.05	0.02	1.08	0.96	0.00	0.96	2.04
0.38	0.01	0.39	0.21	0.00	0.21	0.60
0.49	0.02	0.51	0.38	0.00	0.38	0.90
1.04	0.04	1.08	0.65	0.00	0.65	1.73
1.99	0.05	2.03	1.17	0.00	1.18	3.21
1.05	0.05	1.10	0.79	0.00	0.79	1.89
0.97	0.06	1.03	0.56	0.00	0.56	1.59
1.42	0.06	1.48	0.98	0.00	0.99	2.47
Average	1.24	0.06	1.30	0.93	0.00	0.93	2.22
(± 2σ)	(1.29)	(0.12)	(1.36)	(1.03)	(0.01)	(1.03)	(2.25)

D_T (mGy): Patient thyroid organ doses calculated for DSA and Fluoroscopy (F) runs as a function of the plane. The total D_T for both planes and all runs is also shown.

$$R_P = \frac{Risk_{Age\,Sex}}{(100{,}000\,cases)(100\,mGy)} \times D_T$$

Percentile	D_T	Female				Males			
		25	45	55	65	25	45	55	65
Min	0.35	0.19	0.02	0.01	0.00	0.04	0.01	0.00	0.00
10	0.89	0.48	0.05	0.02	0.01	0.10	0.02	0.00	0.00
30	1.73	0.93	0.10	0.03	0.01	0.19	0.03	0.01	0.00
50	2.17	1.17	0.13	0.04	0.01	0.24	0.04	0.01	0.00
70	2.49	1.34	0.15	0.05	0.02	0.28	0.05	0.01	0.00
90	3.00	1.61	0.18	0.06	0.02	0.34	0.06	0.02	0.01
Max	4.56	2.45	0.27	0.09	0.03	0.51	0.09	0.02	0.01

Patient Risk (R_p): incidence of thyroid cancer per 100,000 cases for female and male patients ages 25 to 65 years using the D_T (mGy) doses calculated in the previous table.